Available online at www.sciencedirect.com
SCIENCE DIRECT
Geochimica et Cosmochimica Acta 70 (2006) 3173–3196
Geochimica
www.elsevier.com/locate/gca

Apatite as a probe of halogen and water fugacities in the terrestrial planets

Alberto E. Patiño Douce *, Michael Roden

Department of Geology, University of Georgia, Athens, GA 30602, USA

Received 8 November 2005; accepted in revised form 28 March 2006

Abstract

Apatite preserves a record of the halogen and water fugacities that existed during the waning stages of crystallization of planetary magmas, when they became saturated in phosphates. We develop a thermodynamic formalism based on apatite–merrillite equilibria that makes it possible to compare the relative values of halogen and water fugacities in Martian, lunar and terrestrial basalts, accounting for possible differences in pressure, temperature and oxygen fugacities among the planets. We show that each of these planetary bodies has distinctive ratios among volatile fugacities at apatite saturation and that these fugacities are in some cases related in a consistent way to volatile fugacities in the mantle magma sources. Our analysis shows that the Martian mantle parental to basaltic SNC meteorites was dry and poor in both fluorine and chlorine compared to the terrestrial mantle. The limited data available from Mars show no secular variation in mantle halogen and water fugacities from ~4 Ga to ~180 Ma. The water and halogens found in present-day Martian surface rocks have thus resided in the planet's surficial systems since at least 4 Ga, and may have been degassed from the planet's interior during a primordial crust-forming event. In comparison to the Earth and Mars, the Moon, and possibly the eucrite parent body too, appear to be strongly depleted not only in H_2O but also in Cl_2 relative to H_2O. Chlorine depletion is strongest in mare basalts, perhaps reflecting an eruptive process characteristic of large-scale lunar magmatism.
© 2006 Elsevier Inc. All rights reserved.

1. Introduction

The influence that water and halogens have on a wide range of planetary properties and processes, such as magma compositions and densities, mantle melting temperatures, the composition of oceans and atmospheres and the occurrence of life, is disproportionate to their low bulk abundances in the terrestrial planets. Fluorine and chlorine are moderately volatile elements that probably condensed in the form of fluorapatite and sodalite, respectively, from the solar nebula (e.g., Fegley and Lewis, 1980; Lodders, 2003). Fluorapatite formed at somewhat lower temperatures (~740 K, Lodders, 2003) than sodalite (~950 K, Lodders, 2003) and in this sense F is slightly more volatile than Cl. The behavior of the two halogens in planetary magmas, however, is distinctly different as Cl partitions into hydrous fluids whereas F partitions into silicate melts (Carroll and Webster, 1994). Thus, Cl is more volatile than F during volcanically driven planetary degassing. Water ice condensed from the solar nebula at much lower temperatures, estimated by Lodders (2003) to be near 200 K. The relative abundances of fluorine, chlorine and water in planetary mantles are thus controlled by, and can yield insight into, the accretionary and early differentiation histories of the planets and their subsequent tectonic and magmatic evolutions.

The focus of this paper is to compare the halogen and water budgets of the mantles of Mars, the Earth, Moon and eucrite parent body. We use a mineralogic probe, apatite, and a thermodynamic treatment of equilibria between apatite and merrillite, a volatile-free phosphate, to constrain the fugacities of F_2, Cl_2 and H_2O in planetary basalts. We show that, even though it is not possible to use results obtained from igneous rocks to estimate absolute

* Corresponding author. Fax: +1 706 542 2425.
E-mail addresses: alpatino@uga.edu (A.E. Patiño Douce), mroden@gly.uga.edu (M. Roden).

0016-7037/$ - see front matter © 2006 Elsevier Inc. All rights reserved.
doi:10.1016/j.gca.2006.03.016

volatile fugacities in planetary mantles, it is feasible to infer the *ratios* between the fugacities of these three volatiles in the mantles of Mars, the Earth, Moon and the eucrite parent body

Apatite has frequently been used to probe the halogen budgets of terrestrial basaltic magmas and their source regions. For example, apatite compositions have been used to infer the complex degassing histories of layered intrusions, and the identity of the dominant halogen. In terrestrial basaltic magmas this is typically F, but in the case of the Stillwater and Bushveld intrusions it is Cl (e.g., Brown and Peckett, 1977; Boudreau and McCallum, 1989; Boudreau et al., 1995; Warner et al., 1998; Willmore et al., 2000). In addition to the evidence from layered intrusions, a variety of apatite compositions (fluor- and chlorapatites) from mantle xenoliths (O'Reilly and Griffin, 2000) also indicate that F_2 and Cl_2 fugacities vary widely in the terrestrial mantle. In contrast to the variability of terrestrial apatites, apatites from the Moon and the SNC meteorites are more homogeneous: lunar apatites are nearly pure fluorapatites whereas Martian apatites have approximately equal amounts of fluor- and chlorapatite components. The lunar and Martian mantles would thus appear to be more homogeneous than the terrestrial mantle in terms of their volatile contents, but of course the sample set for these two planetary bodies is exceedingly small.

In a paper that foreshadowed our application of apatite as a probe of mantle halogen fugacities, Nash and Hausel (1973) used a merrillite–apatite pair in a lunar basalt to infer that F fugacity in lunar magmas was significantly lower than in terrestrial magmas. Our approach differs from that of Nash and Hausel (1973) in several important respects. Most notably we calculate volatile fugacities relative to an apatite–merrillite buffer reaction, rather than absolute fugacities. This methodology makes it possible to account for the large differences in oxygen fugacity between different planetary bodies, which is important because the halogen fugacity required for apatite saturation is controlled by oxygen fugacity. We develop a thermodynamic formalism to estimate relative F_2, Cl_2 and H_2O fugacities from phosphate compositions and apply it to SNC meteorites, terrestrial mafic magmas, lunar rocks, chondritic meteorites and a eucrite. Our analysis leads us to the conclusion that the Martian mantle parental to SNC meteorites is dry and halogen-poor compared to the terrestrial mantle, and that most of Mars' Cl has been stored in the planet's surficial systems since at least 4 Ga. We also suggest that the Moon may be depleted in Cl relative to H_2O, and that this depletion is strongest in mare basalts.

2. Halogen and water contents in the terrestrial planets

2.1. Halogen and water contents in phosphates

The chief halogen and water reservoirs in mafic igneous rocks and their mantle source materials are micas, amphiboles and phosphates (predominantly apatite). Apatite is the most widely distributed of these phases in planetary materials, as it is present in terrestrial, Martian and lunar mafic igneous rocks, basaltic meteorites (eucrites) and primitive meteorites (chondrites and acapulcoites). Phlogopite and amphibole are common in terrestrial igneous rocks, very rare in Martian meteorites and essentially absent from all other planetary materials. Fluorine–potassium relationships (discussed below) show that phlogopite is likely to be an essential reservoir for both of these elements in the Earth's mantle but not in the Martian mantle. Apatite is thus the one phase that can allow a direct comparison of relative halogen and water contents among terrestrial planets. It also provides the basis for quantitative estimates of volatile fugacities in planetary materials.

We have compiled a data base of published phosphate compositions (apatite and merrillite; note that, following Greenwood et al., 2003, we use the latter name to refer to the halogen- and water-free phosphate) from Martian meteorites, lunar rocks, eucrites, various primitive solar system materials (chondrites, acapulcoites and a CAI inclusion) and a number of terrestrial mafic igneous rocks. The sources of data are listed in Table 1, together with calculated mole fractions of halogens, hydroxyl and Ca for apatite and merrillite (Ca mole fractions are included because they are used in the thermodynamic formalism discussed in the next section). Only apatites for which the original source reported both F and Cl values are included in the table. Hydroxyl mole fractions were estimated by difference, assuming that $X_F + X_{Cl} + X_{OH} = 1$. This assumption, which has been made by many previous authors (e.g., Nash, 1976; Brown and Peckett, 1977; Huntington, 1979; Boudreau and McCallum, 1989; Boudreau et al., 1995), relies on two premises: (1) that P does not undergo changes in oxidation state with oxygen fugacity, at least for $f(O_2)$ values in the range of interest for planetary materials (roughly, IW to QFM) and (2) that there are no significant crystallographic vacancies in apatite. Hydroxyl mole fractions calculated by difference are also dependent on analytical accuracy for the halogens and could be affected by large uncertainties, especially in samples in which one of the halogens is present in minor concentrations (e.g., Cl in many lunar rocks). This is an issue to which we will return. We note, however, that measured water contents in apatite in the Martian meteorites Zagami (Watson et al., 1994; McCoy et al., 1999) and ALH84001 (Boctor et al., 2003) are consistent with the mole fractions of OH calculated by difference.

Extraterrestrial samples for which complete apatite analyses (i.e., including halogens) are available are rare. For this reason we were not selective and include in our data set (Table 1) every published extraterrestrial sample with complete apatite analyses that we are aware of. The eucrite data point is rather uncertain, as the values are not an actual analysis but are reconstructed from compositional ranges given by Delaney et al. (1984). In contrast to extraterrestrial samples, the listing of terrestrial rocks is not exhaustive. We chose mafic igneous rocks that represent a

Table 1
Phosphate compositions

Sample	Apatite				Merrillite	Data sources
	X(Ca)	X(F)	X(Cl)	X(OH)[a]	X(Ca)	
Martian meteorites						
Los Angeles	0.983	0.306	0.327	0.367	0.881	Greenwood et al. (2003), Xirouchakis et al. (2002), Mikouchi (2001)
Los Angeles (stone 2)	0.979	0.190	0.393	0.583	0.882	Warren et al. (2004)
Zagami (low Cl)[b]	0.971	0.343	0.342	0.315	0.886	McCoy et al. (1999)
Zagami (high Cl)[b]	1.000	0.341	0.445	0.214	0.886	McCoy et al. (1999)
Shergotty	0.976	0.286	0.413	0.301	0.848	Jagoutz and Wänke (1986)
NWA480	0.956	0.410	0.291	0.298	0.887	Barrat et al. (2002)
Lafayette	0.972	0.433	0.567	0.000		Bunch and Reid (1975)
ALH 84001	0.992	0.250	0.561	0.189	0.851	Greenwood et al. (2003)
ALH 84001	0.989	0.350	0.497	0.153	0.871	Boctor et al. (2003)
EETA79001,357	0.934	0.903	0.086	0.011	0.862	Wang et al. (2004)
Lunar rocks						
Mare basalts						
14053	0.987	0.938	0.023	0.039	0.820	Taylor et al. (2004)
14053	0.996	0.850	0.010	0.140	0.796	Gancarz et al. (1971)
14001,7,3	1.000	0.995	0.005	0.000	0.815	Gancarz et al. (1971)
10002,121	0.982	0.980	0.020	0.000		Beaty et al. (1979)
LAP 02205	0.966	0.513	0.081	0.406		Anand et al. (2006)
Highland rocks						
14310	0.965	0.930	0.043	0.027	0.820	Griffin et al. (1972)
10085-LR-1	0.964	0.753	0.205	0.042	0.773	Albee and Chodos (1970)
14161,7373	0.990	0.803	0.103	0.094	0.795	Jolliff et al. (1993)
14161,7044	1.004	0.803	0.169	0.028	0.784	Jolliff et al. (1993)
14161,7069	0.986	0.660	0.211	0.128	0.768	Jolliff et al. (1993)
14161,7264	0.993	0.940	0.060	0.000	0.765	Jolliff et al. (1993)
14161,7269	0.981	0.766	0.214	0.020		Jolliff et al. (1993)
14161,7350	0.997	0.900	0.100	0.000	0.765	Jolliff et al. (1993)
Impact rocks						
12013,10	0.980	0.718	0.205	0.077	0.768	Lunatic Asylum (1970)
14161,7233	0.986	0.900	0.100	0.000	0.772	Jolliff et al. (1993)
Eucrites						
Delaney et al.	1.000	0.970	0.030	0.000		Delaney et al. (1984)
Chondrites, acapulcoites and related materials						
Seoni	0.954	0.000	0.845	0.155	0.855	Brearly and Jones (1998)
Willowbar	0.983	0.000	0.806	0.194	0.867	Brearly and Jones (1998)
Acapulco (high Cl)[b]	0.969	0.501	0.499	0.000		Min et al. (2003)
Acapulco (high F)[b]	0.989	0.740	0.260	0.000		Min et al. (2003)
Mnmnt Draw (high Cl)[b]	0.982	0.314	0.636	0.051	0.867	McCoy et al. (1996)
Mnmnt Draw (high F)[b]	1.000	0.982	0.018	0.000	0.867	McCoy et al. (1996)
Krymka (high Cl)[b]	0.975	0.298	0.625	0.077	0.833	Semenenko et al. (2004)
Krymka (high F)[b]	0.951	0.658	0.326	0.017	0.833	Semenenko et al. (2004)
Maralinga CAI inclusion	0.978	0.000	0.650	0.000		Kurat et al. (2002)
DaG 896	1.000	0.000	0.661	0.339	0.831	Folco et al. (2004)
Terrestrial igneous rocks[c]						
Stillwater G2	0.999	0.450	0.276	0.274		Boudreau and McCallum (1989)
Stillwater G3	1.000	0.192	0.374	0.434		Boudreau and McCallum (1989)
Kiglaplait OBZ	1.000	0.576	0.116	0.307		Huntington (1979)
Kiglaplait OBZ	1.000	0.635	0.256	0.109		Huntington (1979)
Skaergard CM	0.978	0.703	0.021	0.275		Nash (1976)
Bushveld	0.978	0.000	0.920	0.080		Willmore et al. (2000)
Bushveld	0.993	0.000	0.887	0.113		Willmore et al. (2000)
Great Dyke	0.974	0.472	0.132	0.396		Boudreau et al. (1995)
Sudbury	1.000	0.612	0.181	0.207		Warner et al. (1998)
Sudbury	0.993	0.577	0.191	0.232		Warner et al. (1998)
Mauna Kea xenoliths	0.994	0.867	0.133	0.000		Fodor (2001)
Mauna Kea xenoliths	0.992	0.915	0.085	0.000		Fodor (2001)

(*continued on next page*)

Table 1 (*continued*)

Sample	Apatite				Merrillite	Data sources
	X(Ca)	X(F)	X(Cl)	X(OH)[a]	X(Ca)	
Hess Deep (high F)	0.990	0.718	0.094	0.187		Meurer and Natland (2001)
Hess Deep (low F)	0.994	0.302	0.441	0.256		Meurer and Natland (2001)
Hess Deep (high H_2O)	0.998	0.414	0.273	0.313		Meurer and Natland (2001)
Hawi lavas	0.993	0.947	0.053	0.000		Spengler and Garcia (1988)

[a] X(OH) calculated by difference—see text.
[b] Apatite compositions are variable in these meteorites—chosen values represent typical F- and Cl-rich apatites. Each sample yields a separate set of fugacity values and each calculated fugacity is shown in the figures.

spectrum of magma types and ages and that are, in a broad sense, comparable to basaltic compositions from Mars, the Moon and eucrites. In particular, we chose samples that represent relatively unfractionated terrestrial magmas, so as to avoid complications in halogen contents resulting from extensive fractional crystallization (e.g., Boudreau and McCallum, 1989). Fig. 1 shows all of the apatite analyses listed in Table 1 and also apatite compositions from mantle xenoliths (O'Reilly and Griffin, 2000) which may be representative of some terrestrial basalt source regions.

A noteworthy aspect of the apatites included in our data set is that virtually all of them (except the xenolith apatites) are halogen-rich, with $X_{OH} < 0.5$ and in many cases approaching 0 (Table 1, Fig. 1). Apatites from primitive meteorites, lunar rocks and the eucrite are particularly water poor and many of them could be water-free within analytical uncertainty. Lunar and eucrite apatites are fluorapatites, but those from primitive meteorites range from almost pure fluorapatites to almost pure chlorapatites. We have divided lunar samples into three groups: mare basalts, highland rocks and impact rocks (i.e., rocks that have suffered strong shock effects). With the exception of one mare basalt (the lunar meteorite La Paz Icefield 02205), for which a single apatite analysis is available (Anand et al., 2006), lunar apatites cluster close to the fluorine end-member. The significance of this discordant mare basalt sample, which has a higher halogen deficiency than all other lunar rocks, will likely remain uncertain until further analyses are available. Except for the Type 6 chondrites (Seoni and Willowbar, Table 1) and DaG 896, which contain only Cl-rich apatite, all other samples of primitive solar system material contain both Cl-rich and F-rich apatites (Table 1). Martian apatites are generally Cl-rich but never approach the chlorapatite end-member. With one exception (the Lafayette meteorite) they also appear to be considerably richer in water than lunar and chondritic apatites. The one discordant Martian sample is EETA79001,357, which is near end-member fluorapatite. This data point also reflects a single analysis, so that its significance is not clear. Terrestrial apatites are highly variable and include water-rich apatites, nearly pure fluorapatite similar to lunar apatites, moderately water-rich apatites similar to Martian apatites and nearly pure chlorapatites (Fig. 1). In general, however, fluorapatites tend to dominate among terrestrial mafic igneous rocks.

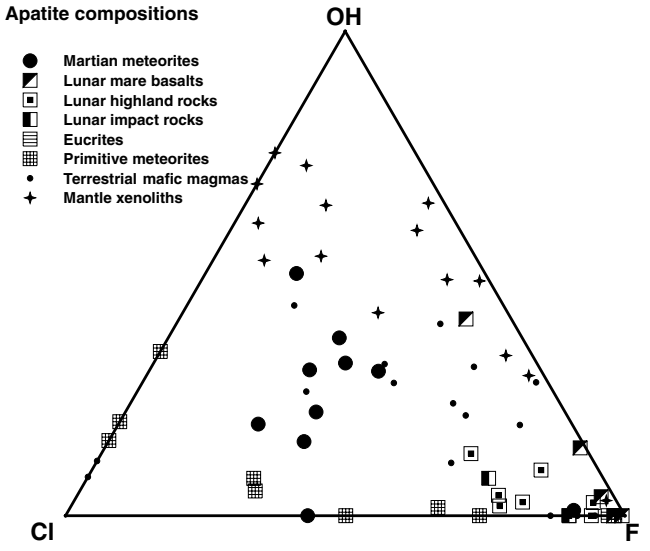

Fig. 1. Volatile components in apatite (molar proportions; data sources and compositions given in Table 1, except for terrestrial mantle xenoliths which are taken from O'Reilly and Griffin (2000)). Mole fractions of OH calculated by difference (see text).

2.2. F and Cl abundances in planetary basalts

Given the striking differences between Martian and lunar apatites and the great variability of terrestrial apatites, it is useful to examine the fluorine and chlorine abundances in planetary basalts to see whether a similar pattern emerges, and to serve as background for the thermodynamic treatment of fluorine and chlorine fugacities in planetary basalts. The geochemistry of these two halogens, however, complicates comparisons of bulk rock chlorine and fluorine contents. Fluorine and chlorine are incompatible elements in basaltic magmas (e.g., Aoki et al., 1981; Jambon et al., 1995) and consequently, concentrations of these halogens will vary with magmatic fractionation. One strategy to avoid the need for fractionation corrections is to index the halogens to another highly incompatible element. Following Aoki et al. (1981) and Jambon et al. (1995), we examine the variations in F and Cl normalized to the highly incompatible element K.

A second important complication is that the halogens are volatile elements and Cl especially can be concentrated in coexisting fluids or vapors (Carroll and Webster, 1994). Consequently, Cl abundances in basalts can decrease significantly if the basalt exsolves a volatile phase (e.g., Unni and Schilling, 1978). For this reason, the terrestrial basalt data that we plot in Figs. 2 and 3 are either from glass inclusions in phenocrysts, submarine glasses erupted at depth (and thus thought to be undegassed) or basalts thought to be undegassed on the basis of other criteria.

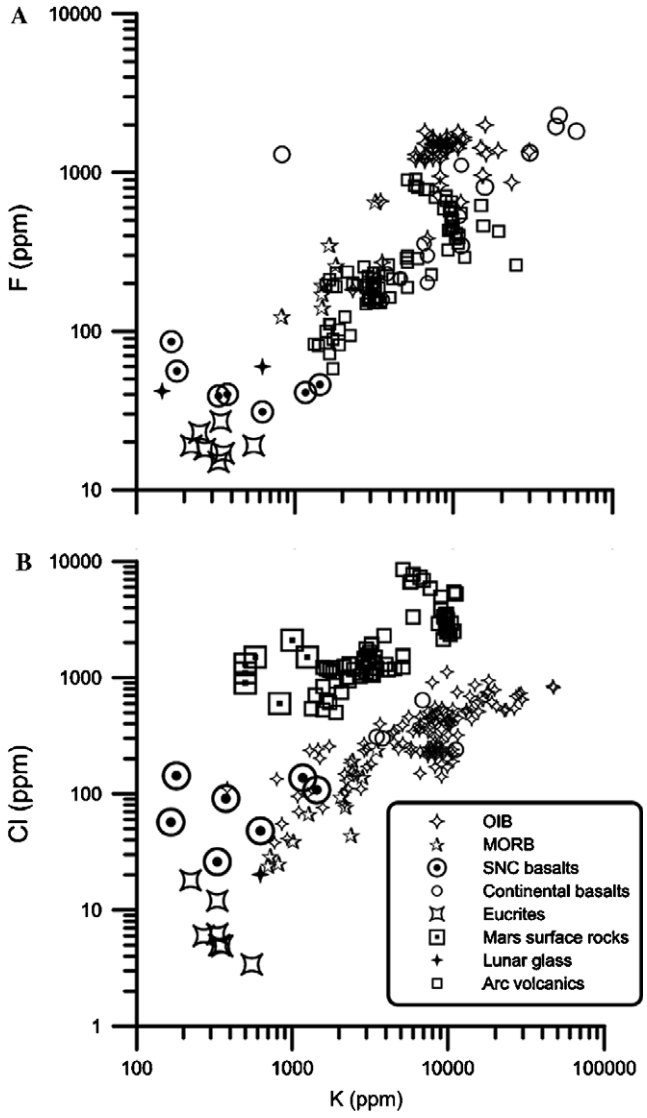

Fig. 2. Plots of F, Cl and K abundances for planetary basalts. Data sources, SNC basaltic meteorites: Lodders (1998), Dreibus et al. (2000, 2003), Meyer (2004); eucrites: Wänke et al. (1972), Basaltic Volcanism Study Project (1981), Mittlefehldt et al. (1998), Sawyer et al. (2000); lunar glasses: Taylor et al. (1991), Mars surface rocks (includes RAT samples and samples corrected for S contents): Gellert et al. (2004), McSween et al. (2004), Rieder et al. (2004); ocean island basalts (OIB): Aoki et al. (1981), Hansteen and Gurenko (1998), McHone (2002), Stroncik and Haase (2004); mid-ocean ridge basalts (MORB): Aoki et al. (1981), Michael and Cornell (averages of ridge localities with mantle Cl/K, 1998); continental basalts: Aoki et al. (1981), McHone (2002); arc volcanics: Aoki et al. (1981), Straub and Layne (2003).

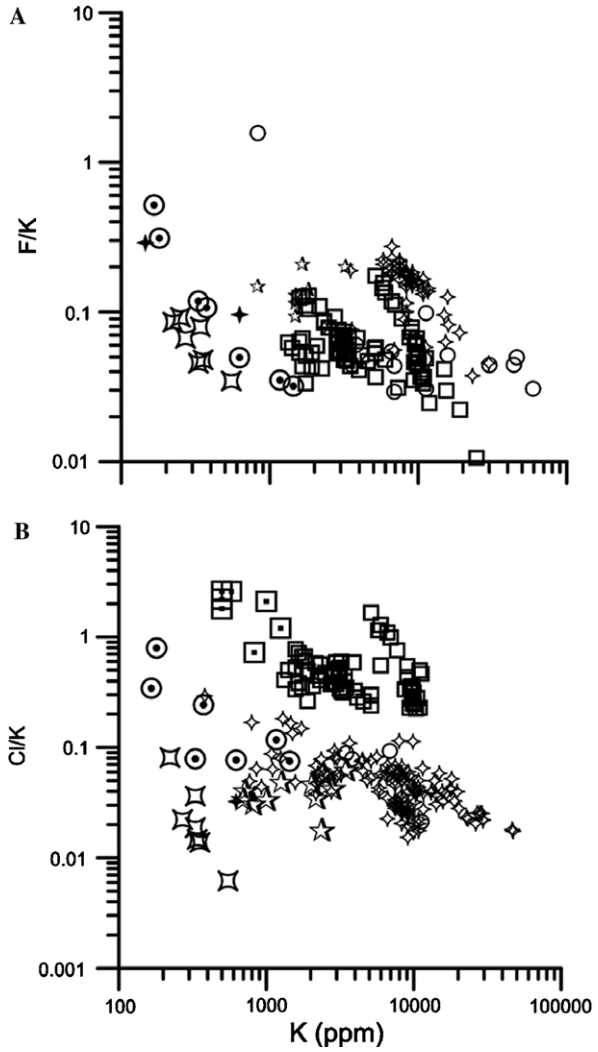

Fig. 3. Plots of F/K and Cl/K versus K. Data sources and symbols as in Fig. 2.

Similar meteorite data, however, are lacking. The SNC and eucrite data are bulk rock data, and at least some SNC's contain halide salts of secondary origin (Bridges and Grady, 1999; Wentworth et al., 2000). Lunar data are from glasses that formed during pyroclastic eruptions (e.g., Taylor et al., 1991) and thus have an uncertain degassing history. We will show below how calculations of volatile fugacities that rely on mineral equilibria make it possible to look through some of these problems, but rock composition data provides the context for those calculations.

The expected incompatible behavior of F and Cl in planetary basalts is illustrated in Fig. 2: F and Cl are positively correlated with K in most basalts, but arc volcanic rocks from the Izu arc show elevated Cl abundances due to recycling of Cl at the arc (Straub and Layne, 2003). Halogen concentrations vary widely: over 3 and 4 orders of magnitude for F and Cl, respectively, with terrestrial basalts ranging to much higher halogen contents than any other basalt. The eucrites are the poorest in halogen contents.

Fluorine/K ratios are independent of K content and most F/K ratios range from about 0.02 to 0.3 (Fig. 3A). In contrast Cl/K ratios are more variable. The spread of Cl/K ratios at relatively high K is due to the recycling of Cl in terrestrial subduction zones (e.g., Straub and Layne, 2003) whereas some of the spread in values at the low K ends of the arrays may be due to degassing of parental magmas or analytical problems with the halogen analyses. For example, measurements of Cl in the eucrite Juvinas range from 5 to 18 ppm and values of Cl/K range from 0.01 to 0.08 (Wänke et al., 1972; Sawyer et al., 2000)—both data points are plotted in Figs. 2 and 3 and show that even given such analytical uncertainty, the eucrites appear to be characterized by very low halogen contents and halogen/K ratios, but the extent to which this is a consequence of degassing during eucrite crystallization versus pre-eruptive parent body degassing remains unknown. Terrestrial basalts are richer in fluorine than any of the extraterrestrial basalts but the SNC basaltic meteorites have bulk Cl contents comparable to those of some terrestrial basalts. Moreover, the SNC basaltic meteorites range to higher values of Cl/K and F/K than MORB and OIB and some SNC basalts have Cl/K ratios comparable to the Izu arc volcanic glasses (Fig. 3B). Mars rover analyses of surface rocks show even higher Cl abundances and range to higher Cl/K ratios than the SNC basaltic meteorites (Figs. 2 and 3B).

To a first approximation, most planetary basalts appear to plot along a single F–K array (Fig. 2) which, although largely defined by terrestrial data, also includes most extraterrestrial samples. Given the strongly incompatible nature of these two elements, the correlation between F and K could indicate that the mantles of the Earth, Moon, Mars and the eucrite parent body had similar contents of volatile F relative to moderately volatile K. The limited data for the shergottites, however, show a distinctive feature: in both the F–K and F/K–K plots, the shergottites define curved arrays that cross the main planetary array. Data for the Moon and eucrite parent body, although consistent with the terrestrial trend, are not sufficient to show whether they also follow a discordant trend in detail.

Terrestrial MORB and OIB define a triangular field in the Cl/K versus K plot (much flattened in this representation because of scale factors) that has been attributed to variable amounts of recycled Cl-rich oceanic crust in the source regions of some OIB (Stroncik and Haase, 2004). The SNC basalts appear to extend the OIB array to higher Cl/K ratios and lower K contents. Mixing models have been proposed to explain observed trace element—isotopic correlations in SNC meteorites (e.g., Borg et al., 2003; Jones, 2005; Warren and Bridges, 2005) and both the F/K–K and Cl/K–K arrays could be viewed as consistent with that idea. If the Cl-rich nature of the Martian surface (e.g., Gellert et al., 2004; Rieder et al., 2004) reflects a characteristic of the entire Martian crust, then one might predict a positive correlation between Cl content, or possibly Cl/K ratio, and a crustal isotopic signature such as initial $^{87}Sr/^{86}Sr$ ratio, but the limited data available (not illustrated) do not show correlations between these parameters. This suggests that Cl enrichment in Mars is restricted to a thin surficial veneer.

The limited SNC basalt data exhibit an inverse correlation between F/K ratio and K content which contrasts with an absence of a correlation between K and F/K in terrestrial basalts. The contrast between Martian and terrestrial basalts is also seen in their absolute F and K contents (Fig. 2). Aoki et al. (1981) suggested that phlogopite is the main mantle host for F and K in the terrestrial mantle and controls F and K abundances in terrestrial basalts. The curved F/K array for the SNC basalts suggests mixing between a relatively high F/K reservoir (crust?) and a low F/K reservoir (mantle?) as the controlling factor in the F/K ratios of Martian basalts. Consequently one major difference between the Earth and Mars is that halogens and alkalis are decoupled in the latter but not in the former. This difference is likely to reflect a hydrous silicate reservoir for halogens and K (phlogopite and/or kaersutite) in the relatively well-mixed terrestrial mantle versus mixing between very old reservoirs largely devoid of hydrous silicates on Mars.

3. Calculation of volatile fugacities in planetary basalts

Volatile contents in planetary samples, including both bulk rock abundances (Figs. 2 and 3) and apatite compositions (Fig. 1), suggest that the Earth, Moon, Mars, and perhaps the eucrite parent body, have variable and possibly different halogen and water budgets. These varying abundances could in turn be reflected in differences in volatile fugacities among the respective planetary mantles. Direct determination of planetary mantle volatile fugacities is hampered by the extreme rarity (except perhaps for the Earth) of appropriate samples, i.e., of mantle assemblages with primary volatile-bearing mineral phases. In contrast, determining the volatile fugacities that prevailed during crystallization of volatile-bearing phases in planetary magmas is possible. These typically late-magmatic fugacities may provide insight about the relationships between water, fluorine and chlorine fugacities in the mantle source regions of basaltic magmas, although not about the absolute values of mantle fugacities. Because apatite is the most widespread volatile-bearing mineral phase in planetary samples we have developed a thermodynamic formalism for estimation of halogen and water fugacities in magmas on the basis of phosphate compositions.

3.1. Thermodynamic formalism and calculations

3.1.1. Definition of log relative fugacities

Apatite is a solid solution of three major end-members, fluorapatite (F-ap), chlorapatite (Cl-ap) and hydroxyapatite (OH-ap). If apatite crystallized at equilibrium with merrillite (as it did in some planetary basalts), then halogen and H_2O fugacities in planetary magmas at the stage at which they became saturated with phosphates can be estimated from the following three equilibria:

$$2[Ca_5(PO_4)_3F]_{ap} + \frac{1}{2}O_2 \rightleftharpoons 3[Ca_3(PO_4)_2]_{me} + [CaO]_{melt} + F_2 \quad (1\text{-F})$$

$$2[Ca_5(PO_4)_3Cl]_{ap} + \frac{1}{2}O_2 \rightleftharpoons 3[Ca_3(PO_4)_2]_{me} + [CaO]_{melt} + Cl_2 \quad (1\text{-Cl})$$

$$2[Ca_5(PO_4)_3OH]_{ap} \rightleftharpoons 3[Ca_3(PO_4)_2]_{me} + [CaO]_{melt} + H_2O \quad (1\text{-OH})$$

Calculation of absolute values of volatile fugacities from the compositions of coexisting apatite and merrillite requires that the phosphates crystallized at equilibrium with silicate–oxide assemblages that fix the chemical potentials of both CaO and O_2. Regardless of whether phosphates coexist with such assemblages, however, it is possible to calculate *relative* fugacity values, measured with respect to reference states given by crystallization of each of the end-member apatites at the same lime activity as the sample of interest and at some arbitrarily chosen oxygen fugacity. Using fluorine as an example, we define log relative fluorine fugacity as follows:

$$\Delta \log f(F_2)_{QFM} = \frac{1}{2}\Delta \log f(O_2)_{QFM} - \log K_{F\text{-phosphates}} \quad (2)$$

with the equilibrium constant given by:

$$K_{F\text{-phosphates}} = \frac{[a(Ca_3(PO_4)_2)_{me}]^3}{[a(Ca_5(PO_4)_3F)_{ap}]^2} \quad (3)$$

(a full derivation of the thermodynamic relations leading to Eq. (2) is given in Appendix A and activity–composition relations are discussed in Appendix B). The variable $\Delta \log f(F_2)_{QFM}$ records the fluorine fugacity under which a given apatite–merrillite assemblage crystallized, measured relative to the fluorine fugacity that would exist at equilibrium between pure end-member fluorapatite and merrillite at the same pressure, temperature and lime activity as the assemblage of interest, and at the oxygen fugacity of the QFM buffer for that pressure and temperature. Log relative chlorine fugacities are defined in an identical manner:

$$\Delta \log f(Cl_2)_{QFM} = \frac{1}{2}\Delta \log f(O_2)_{QFM} - \log K_{Cl\text{-phosphates}} \quad (4)$$

with the equilibrium constant given by:

$$K_{Cl\text{-phosphates}} = \frac{[a(Ca_3(PO_4)_2)_{me}]^3}{[a(Ca_5(PO_4)_3Cl)_{ap}]^2} \quad (5)$$

An important aspect of reactions (1) is that hydroxyapatite stability (at fixed pressure, temperature and CaO activity) is a function of H_2O fugacity only, whereas stability of the other two end-members is a function of oxygen fugacity as well as halogen fugacity (see also Nash and Hausel, 1973; Harrison and Watson, 1984). This crucial difference arises from the need to balance the charge of the Ca^{2+} cation that is transferred from apatite to a silicate phase (melt or solid) when apatite breaks down to merrillite. When hydroxyapatite breaks down the oxygen anion needed to balance Ca^{2+} becomes available from formation of an H_2O molecule. Because halogens do not readily enter anhydrous silicate phases, however, charge balancing of Ca^{2+} from breakdown of halogen apatites requires an externally supplied oxygen anion. In this case oxygen competes with halogens as the Ca oxidant (electron acceptor), leading to the interdependency of halogen and oxygen fugacities (Eqs. (2) and (4)). In contrast, log relative H_2O fugacities do not depend on oxygen fugacity, so the equation becomes (see also Appendix A):

$$\Delta \log f(H_2O) = -\log K_{OH\text{-phosphates}} \quad (6)$$

with:

$$K_{OH\text{-phosphates}} = \frac{[a(Ca_3(PO_4)_2)_{me}]^3}{[a(Ca_5(PO_4)_3OH)_{ap}]^2} \quad (7)$$

Log relative halogen fugacities referred to the QFM oxygen buffer and log relative H_2O fugacities calculated with these equations for the samples listed in Table 1 are given in Table 2 (the choice of oxygen fugacity values for each of the samples is discussed below). Most lunar rocks, Martian meteorites and chondritic materials contain both apatite and merrillite, so that, assuming equilibrium between the two phosphates, Eqs. (2), (4) and (6) yield actual values of log relative fugacities for these samples. Terrestrial rocks, the Lafayette meteorite and lunar samples 10002,121 and 14161,7269 do not contain merrillite. In apatite-bearing but merrillite-free assemblages it is possible to use these equations to calculate *minimum* fugacity values, using an assumed merrillite activity. An assumed value in such case is just a mathematical device and does not imply that the phase merrillite could crystallize in the assemblage under some set of circumstances—in particular, it is legitimate to assume a merrillite activity for terrestrial rocks even if the halogen-poor phosphate found in some terrestrial (non-igneous) rocks is commonly whitlockite and not merrillite (see Dowty, 1977), as long as one keeps in mind the fact that the calculated fugacities are lower bounds and not actual values. Log relative fugacities for Lafayette and for all terrestrial samples were calculated assuming a merrillite activity of 0.65, which is characteristic of Martian meteorites (Appendix B and Table B.1). The choice for Lafayette is obvious. In the case of mafic terrestrial igneous rocks, in which apatite is the only magmatic phosphate, our justification is that Martian basalts are compositionally closer to terrestrial rocks than any of the other samples included in our analysis. We stress that fugacities calculated in this way for terrestrial rocks are likely to be gross underestimations of the real volatile fugacities, but we show later that it is possible, even in the absence of merrillite, to obtain absolute comparisons of volatile fugacity *ratios* among the various planetary bodies. Fugacities for lunar samples 10002,121, 14161,7269

Table 2
Calculated relative volatile fugacities and equilibrium constants[a]

	log K[b]			Volatile relative fugacities		
	F-ph	Cl-ph	OH-ph	$\Delta\log f(F_2)_{QFM}$	$\Delta\log f(Cl_2)_{QFM}$	$\Delta\log f(H_2O)$
Martian meteorites[c]						
Los Angeles	0.605	0.548	0.448	−1.21	−1.15	−0.45
Los Angeles (stone 2)	1.044	0.413	0.070	−1.64	−1.01	−0.07
Zagami (low Cl)	0.582	0.585	0.656	−1.18	−1.18	−0.66
Zagami (high Cl)	0.461	0.230	0.866	−1.06	−0.83	−0.87
Shergotty	0.550	0.231	0.505	−1.15	−0.83	−0.51
NWA480	0.503	0.800	0.780	−1.10	−1.40	−0.78
Lafayette	*0.379*	*0.145*		*−0.98*	*−0.74*	
ALH 84001	0.609	−0.093	0.852	−1.21	−0.51	−0.85
ALH 84001	0.433	0.128	1.152	−1.03	−0.73	−1.15
EETA79001,357	−0.195	1.847	3.634	−0.41	−2.46	−3.63
Mean[d]	0.578	0.289				
s.d.[d]	0.173	0.279				
Lunar rocks[e]						
Mare basalts						
14053	−0.663	2.558	2.099	−1.84	−5.06	−2.10
14053	−0.736	3.123	0.831	−1.76	−5.62	−0.83
14001,7,3	−0.797	3.801		−1.70	−6.30	
10002,121	*−0.810*	*2.575*		*−1.69*	*−5.07*	
LAP 02205	*−0.171*	*1.432*	*0.032*	*−2.33*	*−3.93*	*−0.03*
Mean[d]	−0.635	2.698				
s.d.[d]	0.238	0.779				
Highland rocks						
14310	−0.560	2.110	2.514	−1.94	−4.61	−2.51
100085-LR-1	−0.601	0.529	1.906	−1.90	−3.03	−1.91
14161, 7373	−0.662	1.122	1.202	−1.84	−3.62	−1.20
14161,7044	−0.781	0.572	2.134	−1.72	−3.07	−2.13
14161,7069	−0.611	0.379	0.813	−1.89	−2.88	−0.81
14161,7264	−0.961	1.429		−1.54	−3.93	
14161,7269	*−0.587*	*0.520*	*2.579*	*−1.91*	*−3.02*	*−2.58*
14161,7350	−0.942	0.967		−1.56	−3.47	
Mean[d]	−0.713	0.954				
s.d.[d]	0.151	0.552				
Impact rocks						
12013,10	−0.653	0.436	1.286	−1.85	−2.94	−1.29
14161,7233	−0.857	1.051		−1.64	−3.55	
Mean[d]	−0.755	0.744				
s.d.[d]	0.102	0.308				
Eucrites[f]						
Delaney et al.	*−0.877*	*2.143*		*−1.37*	*−4.39*	
Chondrites and acapulcoites[g]						
Seoni		−0.262	1.211		−1.99	−1.21
Willowbar		−0.295	0.942		−1.96	−0.94
Acapulco (high Cl)	*0.178*	*0.181*		*−2.43*	*−2.43*	
Acapulco (high F)	*−0.253*	*0.656*		*−2.00*	*−2.91*	
Mnmnt Draw (high Cl)	0.526	−0.087	2.104	−2.78	−2.16	−2.10
Mnmnt Draw (high F)	−0.544	2.930		−1.71	−5.18	
Krymka (high Cl)	0.447	−0.196	1.623	−2.70	−2.05	−1.62
Krymka (high F)	−0.130	0.480	3.046	−2.12	−2.73	−3.05
Maralinga CAI inclusion		−0.092			−2.16	
DaG 896		−0.362	0.218		−1.89	−0.22
Terrestrial samples[h]						
Stillwater G2	*0.195*	*0.619*	*0.626*	*−0.19*	*−0.62*	*−0.63*
Stillwater G3	*0.931*	*0.352*	*0.223*	*−0.93*	*−0.35*	*−0.22*
Kigaplait OBZ	*−0.023*	*1.369*	*0.523*	*0.02*	*−1.37*	*−0.52*
Kigaplait OBZ	*−0.108*	*0.681*	*1.423*	*0.11*	*−0.68*	*−1.42*
Skaergard CM	*−0.102*	*2.948*	*0.714*	*0.10*	*−2.95*	*−0.71*
Bushveld		*−0.333*	*1.788*		*0.33*	*−1.79*

Table 2 (*continued*)

	log K[b]			Volatile relative fugacities		
	F-ph	Cl-ph	OH-ph	$\Delta\log f(F_2)_{QFM}$	$\Delta\log f(Cl_2)_{QFM}$	$\Delta\log f(H_2O)$
Bushveld		*−0.370*	*1.420*		*0.37*	*−1.42*
Great Dyke	*0.262*	*1.369*	*0.415*	*−0.26*	*−1.37*	*−0.41*
Sudbury	*−0.076*	*0.982*	*0.866*	*0.08*	*−0.98*	*−0.87*
Sudbury	*0.007*	*0.967*	*0.798*	*−0.01*	*−0.97*	*−0.80*
Mauna Kea xenoliths	*−0.353*	*1.275*		*0.35*	*−1.28*	
Mauna Kea xenoliths	*−0.392*	*1.672*		*0.39*	*−1.67*	
Hess Deep (high F)	*−0.169*	*1.597*	*0.999*	*0.17*	*−1.60*	*−1.00*
Hess Deep (low F)	*0.565*	*0.237*	*0.709*	*−0.57*	*−0.24*	*−0.71*
Hess Deep (high H_2O)	*0.271*	*0.633*	*0.514*	*−0.27*	*−0.63*	*−0.51*
Hawi lavas	*−0.424*	*2.080*		*0.42*	*−2.08*	

Samples are arranged in the same order as in Table 1.

[a] Values in italics are for samples that do not contain merrillite. They are either minimum values or approximate values—see text.

[b] Equilibrium constants calculated with Eqs. (3), (5) and (7) and end-member activities from Table 1.

[c] Halogen fugacities for all Martian samples calculated at $f(O_2) = QFM—1.2$.

[d] Mean and standard deviations of equilibrium constants of Martian and lunar samples, used to plot mean halogen-oxygen lines with Eqs. (2) and (4). See text and Figs. 4 and 5. Martian average excludes EETA79001,357 (see text).

[e] Halogen fugacities for all lunar samples calculated at $f(O_2) = QFM—5.0$.

[f] Halogen fugacities for the eucrite calculated at $f(O_2) = QFM—4.5$.

[g] Halogen fugacities for all primitive meteorites calculated at $f(O_2) = QFM—4.5$.

[h] Halogen fugacities for all terrestrial samples calculated at $f(O_2) = QFM$.

and LAP 02205 (the latter contains merrillite but no analyses are available) were calculated assuming a merrillite activity of 0.5, which is an average value for lunar rocks. The lower merrillite activity in lunar rocks compared to Martian meteorites reflects the higher REE content of lunar phosphates.

Merrillite has been reported in eucrites and in the Acapulco meteorite (Table 1), but we are not aware of any published merrillite compositions for either of these sample groups. We therefore calculated log relative fluid fugacities for these samples with assumed merrillite activities of 0.5 and 0.65 for eucrites and the Acapulco meteorite, respectively. These are characteristic merrillite activities in samples that may be comparable to eucrites and Acapulco, namely, lunar basalts and chondritic meteorites, respectively. In this case the calculated volatile fugacities are not minimum values but rather rough estimates.

3.1.2. Log relative fugacities and absolute volatile fugacities

Variations in log relative fugacities calculated from different rocks that contain both phosphates in equilibrium reflect the differences in the corresponding absolute volatile fugacities between the rocks, except for the effects of intersample variations in lime activity. This is shown by the following equation which relates absolute and relative fluorine fugacities for two putative samples (labeled 1 and 2) that equilibrated at the same temperature and pressure but at possibly different oxygen fugacities and lime activities (complete derivation is given in Appendix C):

$$\log f(F_2)_1 - \log f(F_2)_2 = \Delta\log f(F_2)_{QFM,1} - \Delta\log f(F_2)_{QFM,2} - \log\left[\frac{a(CaO)_1}{a(CaO)_2}\right] \quad (8)$$

Eq. (8) shows that, if a fixed oxygen fugacity reference is used, then the *difference* between log relative halogen (and water) fugacities (e.g., $\Delta\log f(F_2)_{QFM}$) calculated for any two apatite–merrillite assemblages *that crystallized under the same lime activity*, *temperature and pressure* exactly tracks the difference between the respective log absolute halogen fugacities under which those apatite–merrillite assemblages crystallized. Of course, temperature, pressure and lime activity are likely to differ among samples so it is necessary to assess how this variability can affect the significance of calculated log relative fugacities. The effect of changes in lime activity is evaluated in Appendix C and Table C.1. The range in mineral compositions among Martian and lunar samples results in a maximum value for the logarithm of the ratio of lime activities (the last term in Eq. (8)) of ± 0.25 log units. In particular, there appears to be little, if any, significant difference between lime activities in lunar and Martian rocks (Table C.1), even though the Martian samples in the table include basaltic shergottites and a clinopyroxenite, and lunar rocks include KREEP basalts and a quartz-monzodiorite. For a fairly wide range in mafic bulk compositions, then, the extent to which differences among log relative fugacities are likely to depart from differences among absolute fugacities is comparable to the uncertainty that can be expected from analytical errors (see Appendix D). The effect of lime activity changes could be greater when comparing a less mafic rock (e.g., lunar felsite 14161,7269) to a basaltic rock. With decreasing lime activity the calculated log relative fugacities would decrease relative to the values shown in Table 2. This effect, however, would have the same magnitude for all three volatiles, so it cannot be the reason behind the contrasting behaviors of fluorine and chlorine fugacities (see below).

It also follows immediately from Eq. (2) that the effect of temperature and pressure uncertainties on log relative halogen fugacities is given by:

$$\Delta \log f(\mathrm{F_2})_{\mathrm{QFM},T_1P_1} - \Delta \log f(\mathrm{F_2})_{\mathrm{QFM},T_2P_2} = \frac{1}{2}\left[\Delta \log f(\mathrm{O_2})_{\mathrm{QFM},T_1P_1} - \Delta \log f(\mathrm{O_2})_{\mathrm{QFM},T_2P_2}\right] \quad (9)$$

where T_1, P_1 and T_2, P_2 are two arbitrary sets of conditions under which a given assemblage could have crystallized. This equation shows that, if a mineral assemblage crystallized on the QFM oxygen buffer, or along another buffer that exactly parallels the QFM buffer in P-T-$f(\mathrm{O_2})$ space, then, because the quantity $\Delta \log f(\mathrm{O_2})_{\mathrm{QFM}}$ is, by definition, a constant, independent of pressure and temperature, log relative halogen fugacities calculated relative to the QFM oxygen buffer would be unaffected by temperature and pressure uncertainties. This may be a reasonable approximation for many Martian and terrestrial samples. Lunar rocks appear to have been buffered close to either an iron-silicate buffer (Nash and Hausel, 1973) or an iron-graphite-oxide-CO_2 buffer (Sato, 1978; Taylor, 1982). In such cases an uncertainty in $\Delta \log f(\mathrm{F_2})_{\mathrm{QFM}}$ of the order of 0.25 log units (i.e., comparable to the uncertainties derived from possible differences in lime activity) would arise from temperature variations of ~200 °C or pressure variations of ~8 kbar. Because phosphates are always late crystallizing phases in planetary basalts (Huntington, 1979; Boudreau and McCallum, 1989; Sha, 2000; Xirouchakis et al., 2002; Greenwood et al., 2003) the temperature interval under which they typically form may be of this order, whereas pressures in volcanic and subvolcanic systems will vary over ranges much smaller than 8 kbar. We note, nevertheless, that whatever uncertainties may arise from lack of pressure and temperature constraints would affect calculations of absolute halogen fugacities to the same extent.

This discussion shows that differences in the volatile fugacities that existed when phosphates crystallized in different samples can be estimated by means of log relative halogen and water fugacities, as defined by Eqs. (2), (4) and (6). An altogether different question is the extent to which these log relative volatile fugacities, which typically reflect conditions at a late stage in the crystallization of planetary magmas, may preserve a memory of the primary volatile fugacities in planetary mantles. In order to discuss this crucial issue it is necessary to first look at oxygen fugacities in the terrestrial planets.

3.2. Oxygen fugacity in planetary basalts

Because oxygen fugacity is one of the intensive variables that controls crystallization of halogen apatites (see reactions (1-F) and (1-Cl)) it is necessary to know its value in order to calculate halogen fugacities. Note that, whereas oxygen fugacity determines the halogen fugacity that is required for apatite crystallization, and may fix halogen fugacities once the full buffering assemblage is present (see, for example, Eqs. (1-F) and (2)), changes in melt oxygen fugacity that take place before apatite crystallizes will not affect melt halogen fugacities. This is so because in the absence of a solid buffering assemblage (such as the two-phosphate assemblages in Eqs. (1)) halogen and oxygen fugacities are decoupled. Crystallization of halogen-bearing silicates (e.g., mica or amphibole) before phosphates could invalidate this argument but, as we discuss below, such crystallization is rare. The oxygen fugacity values that we use in our calculations, which appear to be generally agreed upon values for crystallization of basaltic magmas in the various planetary bodies, are discussed in the following paragraphs.

Of the six Martian meteorites included in our analysis, three (Los Angeles, Zagami and Shergotty) have oxide-silicate assemblages that allow straightforward estimation of $f(\mathrm{O_2})$. Herd et al. (2001) obtained consistent $f(\mathrm{O_2})$ values for these three meteorites in the range QFM-1.6 to QFM-1.0, and Xirouchakis et al. (2002) estimated that the last stages of crystallization of Los Angeles occurred close to QFM-1. We have adopted an intermediate value of QFM-1.2 as typical of these three shergottites. Oxygen fugacities during crystallization of the other three Martian meteorites are less well known. Reported oxide analyses for Lafayette (titanomagnetite, Bunch and Reid, 1975) and ALH84001 (chromite, Mittlefehldt, 1994) contain substantial amounts of Fe^{3+}, suggesting that these cumulate rocks are unlikely to have crystallized under more reducing conditions than the basaltic shergottites, but we are unaware of any more precise estimate of the oxidation states of these two meteorites. The oxide assemblage of NWA480 (another shergottite) consists of ilmenite and chromite (Barrat et al., 2002), which does not yield reliable $f(\mathrm{O_2})$ estimates. In the absence of other constraints we assume that $f(\mathrm{O_2})$ for these other three Martian samples was also QFM-1.2. We adopted an oxygen fugacity value for all lunar rocks of QFM-5 (≈IW-1.5). This value is consistent with recent reviews by Delano (2004) and Shearer and Papike (2004) who show that multiple lines of evidence (e.g., presence of metallic Fe and absence of Fe^{3+}, low oxidation state of polyvalent elements such as Ti, Cr, Eu and V, and experimental studies of lunar basalts) converge on redox conditions for the lunar interior in the range IW-0.5 to IW-2.2. Jones (2004a) has reviewed the evidence for the oxidation conditions of several types of meteorites and concluded that the eucrite parent body, ordinary chondrites and acapulcoites are all likely to have formed under $f(\mathrm{O_2})$ in the neighborhood of IW-1. We have therefore adopted a value of QFM-4.5 for the eucrite and for the primitive solar system materials listed in Table 1. Finally, we assumed that all terrestrial samples equilibrated at QFM. This is admittedly an oversimplification, as there are likely to be significant variations among the samples included in our analysis. However, given that halogen and water fugacity estimates for terrestrial samples are only lower bounds (because of the absence of merrillite), we argue that more precise estimates of oxygen fugacity would not lead to any meaningful additional information.

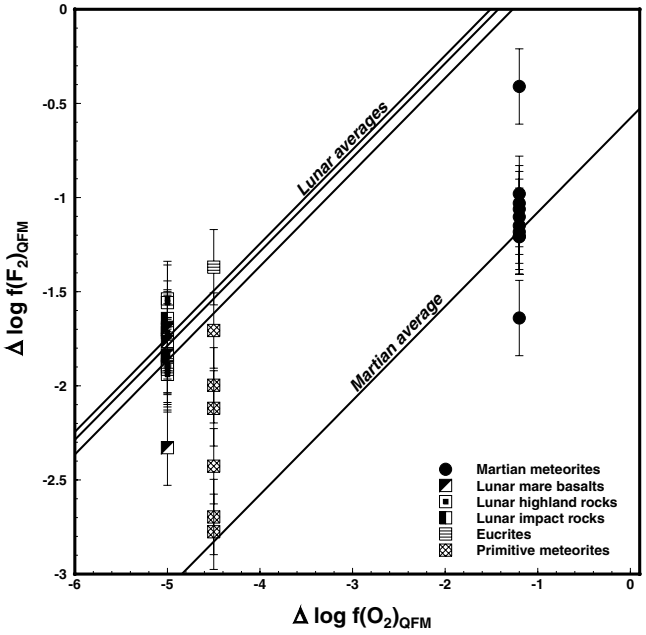

Fig. 4. Relationship between relative fluorine and oxygen fugacities. The solid lines labeled "averages" are plots of Eq. (2) with log $K_{F\text{-phosphates}}$ equal to the mean for all Martian samples and for the three groups of lunar samples (values listed in Table 2). Uncertainties in the averages (±1 standard deviations, listed in Table 2) are of the order of 0.15–0.25 log units.

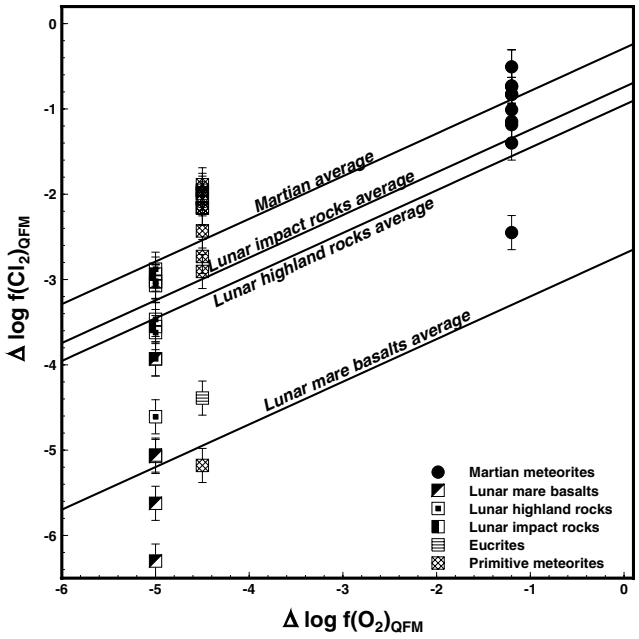

Fig. 5. Relationship between relative chlorine and oxygen fugacities. Details as for Fig. 4. Uncertainties in the averages (±1 standard deviations, listed in Table 2) are of the order of 0.8 log units for mare basalts and 0.3–0.55 log units for other lunar rocks and Martian meteorites.

QFM-based relative halogen fugacities for the Moon are lower than those for Mars (Table 2), implying that absolute fluorine and chlorine fugacities when apatite crystallized were lower in the Moon than in Mars (see Eq. (8)). This is perhaps not an unexpected conclusion (Nash and Hausel, 1973, noted the relatively low F fugacities in lunar basalts), but when relative halogen fugacities are compared in the light of the difference in oxygen fugacity between the two planetary bodies a more complex relationship appears. This relationship can be examined by plotting $\Delta \log f(F_2)_{QFM}$ against $\Delta \log f(O_2)_{QFM}$ (Fig. 4). The straight lines (labeled "averages") were plotted by applying the average values of $K_{F\text{-phosphates}}$ for all Martian samples and for each of the three groups of lunar samples (given in Table 2) to Eq. (2). These lines track the possible combinations of fluorine and oxygen fugacities that could have caused apatite saturation in each planetary body (the three lunar averages are probably statistically indistinguishable, see standard deviations in Table 2). It is clear that, regardless of possible uncertainties in the oxidation states of the two bodies (and of the actual oxidation state of individual samples such as Lafayette, ALH84001 or Los Angeles), the ratios of fluorine to oxygen fugacities during apatite crystallization in the Moon and Mars were distinctly different. For example, if oxygen fugacity when apatite crystallized in the Moon and Mars had been the same, then the fluorine fugacities during apatite crystallization would have been ~1.5 log units higher in the Moon than in Mars. There are several possible factors (not mutually exclusive) that may account for this contrast, including differences in temperature, pressure and relative concentrations of fluorine, chlorine and water in the residual melts that become saturated in phosphates (note that differences in phosphorus activity can be ruled out, as this intensive variable is buffered in lunar and Martian basalts by the presence of merrillite).

Chlorine–oxygen relationships (Fig. 5, plotted by applying the average values of $K_{Cl\text{-phosphates}}$ to Eq. (4)) do not follow the same pattern as fluorine–oxygen relationships. There is little overlap between the lunar and Martian sample sets. Chlorine fugacities during apatite crystallization were lower in the Moon relative to Mars not only in absolute terms but also if the oxygen fugacity difference between the two planets were to be removed (Fig. 5). Lunar mare basalts yield chlorine fugacities that are significantly lower than those in lunar highland rocks and impact rocks. The single eucrite data point, albeit very uncertain, appears to be comparable to mare basalts in terms of both F–O and Cl–O relationships. Primitive solar system materials display a wide range in fluorine and halogen fugacities which, however, does not extend much beyond the range defined by the lunar and Martian averages.

3.3. Do volatile fugacities in planetary basalts reflect fugacities in planetary mantles?

Phosphates are commonly late crystallizing phases in basaltic planetary magmas. This is evident from textural relationships (e.g., Mikouchi, 2001; Xirouchakis et al., 2002; Warren et al., 2004) and is further supported by

the fact that P abundances in unfractionated basalts are lower than those required for phosphate saturation, especially at the low oxygen fugacities characteristic of lunar and Martian magmas (e.g., Toplis et al., 1994; Sha, 2000). An important question is, thus, the extent to which the late-stage volatile fugacities that are recorded in apatite preserve some memory of volatile fugacities in the mantle sources of planetary basalts.

If a planetary basalt evolves by fractional crystallization only and does not become saturated in other volatile-bearing (solid or gas) phases before apatite, then the volatile concentrations in the residual melt that crystallizes apatite are simply related to the volatile concentrations in the primary melt by an enrichment factor equal to the inverse of the fraction of remaining melt. Because it is seldom possible to calculate this fraction with any degree of certainty, estimating initial volatile fugacities from fugacities measured at apatite saturation is not simple. If apatite is the first volatile-bearing phase to crystallize, however, the concentrations of halogens and water in the residual melt will all have increased by the same factor relative to their respective abundances in the primary melt that last equilibrated with its source. One may thus expect that, under such conditions, the *ratios* between volatile fugacities at apatite saturation are related in some simple and predictable way to the fugacity ratios of the primary melt and, hence, to the fugacity ratios at the source of the melt.

In this simple end-member case, the ratio between the fugacities of two volatile species, a and b, in the primary melt (f^i) is related to the fugacity ratio recorded at apatite saturation (f^s) by the following expression (see derivation in Appendix E):

$$\frac{f_a^i}{f_b^i} = \frac{f_a^s}{f_b^s} \cdot \left[\frac{k_a^i/k_a^s}{k_b^i/k_b^s}\right] \cdot \left[\frac{f_a^{o,i}/f_a^{o,s}}{f_b^{o,i}/f_b^{o,s}}\right] \quad (10)$$

where k are Henry's law constants for dissolution of halogens and water in silicate melts and f^o are standard state fugacities, at the conditions at which the primary melt separated from its source (i) and at the conditions at which apatite crystallized (s). Lacking actual values for the individual Henry's law constants (and their pressure and temperature dependencies) we assume that the *ratios* between Henry's law constants are themselves constant (although not necessarily equal to one) for each volatile pair. If this assumption is correct than the ratio of fugacities at the source is proportional to the ratio of fugacities at apatite saturation and to the ratio of standard state fugacities, which can be calculated from equations of state. Standard state fugacity ratios (the last term in Eq. (10)) are shown in Fig. 6 for various volatile pairs as a function of the pressure of formation of the primary melt, assuming that melting occurred at 1300 °C and that apatite crystallized at low pressure (1 bar) and 900 °C (calculation details are given in the figure caption). Extrapolation of the halogen results to pressures greater than a few kbar is very uncertain, so that Fig. 6 should not be taken to represent a precise quantitative result. The plot does suggest, however, that the ratios of Cl_2 to F_2 and H_2O to F_2 fugacities in the mantle source regions of basaltic melts may be higher and lower, respectively, than the corresponding fugacity ratios recorded in late-crystallizing apatite–merrillite pairs (note that the contrasting behaviors of Cl_2 and H_2O relative to F_2 become apparent from the lowest pressures, at which the equations of state are more trustworthy). The crucial point is that, if apatite is the first volatile-bearing phase (solid or gas) to saturate a basaltic melt, then the ratios of Cl_2 to F_2 to H_2O fugacities recorded in apatite are related in a consistent and predictable way to the corresponding fugacity ratios of the primary magma. If this primary magma equilibrated with its source then this will also be the fugacity ratio in the mantle source *when melt separation took place*.

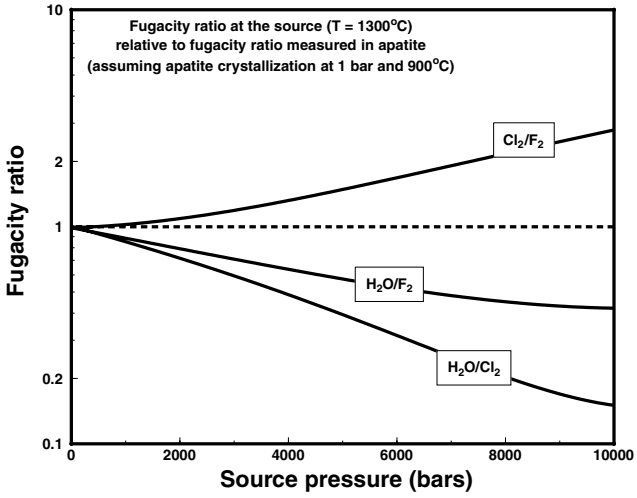

Fig. 6. Change in standard state fugacity ratios between a source at 1300 °C and variable pressure, and "late magmatic" conditions of 1 bar and 900 °C, assumed to correspond to phosphate crystallization conditions (see Eq. (10)). Standard state fugacities were calculated with the Redlich–Kwong equation of state. Redlich–Kwong constants for H_2O were taken from Holloway (1987), and those for F_2 and Cl_2 were calculated (using the theory of corresponding states) from the critical gas constants given by Mathews (1972).

In order for this conclusion to be valid, melts must evolve by fractional crystallization only and must not become saturated in other volatile-bearing minerals nor in a vapor phase before apatite crystallizes. Lunar and Martian basalts characteristically do not contain volatile-bearing mineral phases other than apatite, and this is also true of most terrestrial mid-ocean ridge basalts, ocean island basalts and continental flood basalts. The available Martian basalts (and associated cumulate mafic rocks) do not generally show evidence of having evolved a volatile phase. The terrestrial samples that we include in our analysis represent a wide range of intrusive and subvolcanic lithologies (Table 1). For layered intrusions we chose samples from early, relatively unfractionated units which may not have undergone degassing. MORB samples, in contrast, may have been influenced by degassing and/or post-eruptive fluid activity, and this is probably reflected in their variable halogen-water contents (see Hess Deep samples in Tables 1 and 2). Lunar samples may have also undergone degas-

sing, given the fact that many mare basalts are vesicular, that the presence of glass spherules in the lunar regolith provides evidence for lava fountaining, and that some lunar rocks have undergone impact melting. Magma degassing leads to preferential chlorine and water loss, whereas fluorine tends to stay dissolved in the silicate melt (Candela, 1986; Carroll and Webster, 1994). The tight clustering of fluorine fugacities in both Martian and lunar samples, and the wider spread of chlorine (and perhaps water) fugacities among lunar samples than Martian samples (Figs. 4 and 5, see also below), are thus consistent with different volatile saturation histories of lunar and Martian samples, in which lunar samples have undergone more extensive and complex degassing histories than SNC meteorites. We argue that the ratios among volatile fugacities calculated from SNC meteorites are related in a consistent way to the corresponding fugacity ratios in the Martian mantle. For lunar rocks the situation may be more complicated. We will show later that many lunar rocks, most notably mare basalts, appear to record Cl_2/H_2O fugacity ratios that are significantly lower than those found in Martian and terrestrial rocks. This observation must be considered as tentative, as it relies on OH contents in apatite calculated by difference, but, if it proves to be true, then it points to chlorine/water fractionation either in the source of mare basalts or during mare volcanism.

Another process that could affect the relationship between volatile fugacities recorded in apatite and mantle source fugacities is devolatilization during shock metamorphism. The two lunar impact rocks provide circumstantial evidence that this is not a serious concern. These two rocks are shocked highland lithologies, yet their calculated fluorine and chlorine fugacities do not differ significantly from those of more pristine highland rocks (Table 2, Figs. 4 and 5, see also below). One can infer from this observation that, as long as apatite crystals survive shock metamorphism, they remain essentially closed to volatile exchange.

A final point that must be made is that the discussion in this section applies only to halogens and water, and not to oxygen. During fractional crystallization, oxygen fugacity changes in response to the Fe^{3+}/Fe^{2+} ratio of the fractionating mineral assemblage but, in the absence of a buffering assemblage (such as Eqs. (1)), oxygen fugacity is decoupled from halogen fugacities.

4. Discussion of thermodynamic results

Relative halogen and water fugacities (Table 2) make it possible to compare the absolute volatile fugacities at apatite saturation in the various planetary bodies, because differences in relative fugacities track the differences in the respective absolute fugacities at apatite saturation (see Eq. (8)). Calculated fugacities (both relative and absolute) are of course the actual values of these variables only for samples in which co-crystallization of two phosphates took place. This is probably true of most lunar rocks and Martian meteorites. Many primitive solar system materials also contain apatite and merrillite, but whether the two phosphates crystallized at equilibrium is highly uncertain. For terrestrial rocks, which do not contain merrillite, the relative fugacity values shown in Table 2 are only lower bounds, as discussed above (see Eq. (1)).

Among lunar rocks and Martian meteorites, $\Delta\log f(F_2)_{QFM}$ is virtually constant, with a variability that

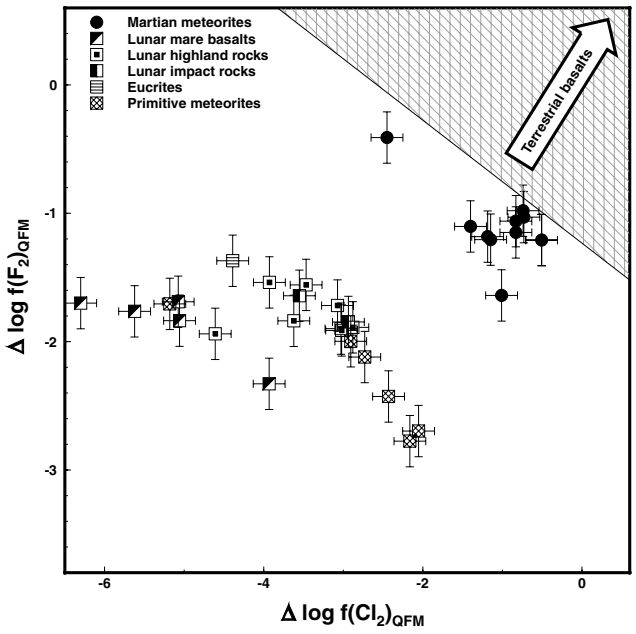

Fig. 7. Relationship between relative fluorine and chlorine fugacities (see Table 2). Terrestrial igneous rocks do not contain merrillite, so it is possible to calculate only minimum values for $\Delta\log f(F_2)_{QFM}$ and $\Delta\log f(Cl_2)_{QFM}$. The stippled area represents the range in these minimum values (shown in Table 2).

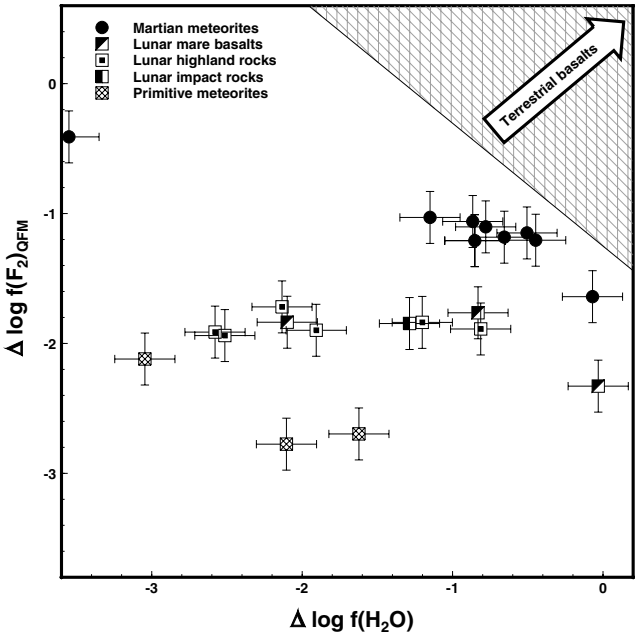

Fig. 8. Relationship between relative fluorine and water fugacities. Details as for Fig. 7.

may not exceed the uncertainty in the calculations (Figs. 7 and 8). Fluorine fugacities in the three groups of lunar rocks are generally indistinguishable from one another. The two notable outliers among Martian rocks are stone 2 of the Los Angeles meteorite, which yields a lower fluorine fugacity than all other Martian meteorites, and EETA79001,357, which yields significantly higher fluorine fugacity. The significance of these outliers is not clear, because in both cases the fugacity values are based on a small number of analyses of single apatite grains. On average, apatite crystallization in the Moon occurred under fluorine fugacities that were approximately half a log unit lower than those under which apatite crystallized in Martian rocks, but under distinctly higher fluorine to oxygen fugacity ratios than in Mars (Fig. 4). Martian and lunar data points in Figs. 7 and 8 cannot be made to overlap even if different estimates of oxygen fugacities were applied to the two planets.

Our interpretation of the constancy of fluorine fugacities is that fluorine fugacity determined the onset of apatite crystallization in lunar and Martian rocks. A reason why this may have been the case is that, if apatite follows the behavior of other halogen- and water-bearing compounds, then fluorapatite must have a significantly higher thermal stability than both chlorapatite and hydroxyapatite. The stabilizing effect of F on apatite at magmatic temperatures was noted by Beswick and Carmichael (1978) and is also consistent with the phase equilibrium analysis of Tacker and Stormer (1993). If our interpretation is correct, then the constancy of calculated fluorine fugacities in the Moon and Mars implies that merrillite was the first phosphate phase to crystallize, and apatite crystallization followed when a critical ratio of fluorine to oxygen fugacity was attained during magmatic crystallization. This can be seen in a schematic phase diagram that maps crystallization of merrillite and apatite as a function of the activity of P_2O_5 in the melt and the ratio of fluorine to oxygen fugacities in the melt (Fig. 9, which shows isothermal and isobaric phase relations for end-member fluorapatite as an example). Crystallization of phosphates in the Moon and Mars probably followed a path such as A in the diagram. Fractional crystallization would have raised the activities of P_2O_5 and F_2 in the melt until the merrillite phase boundary was intersected. When merrillite crystallizes it buffers the activity of P_2O_5 (as long as the silicate assemblage buffers the activity of CaO, which is probably a reasonable approximation, see Appendix C) and further fractional crystallization causes F_2 fugacity, but not P_2O_5 activity, to increase, resulting in a horizontal path along the merrillite phase boundary. When the melt becomes saturated in apatite at the pseudoinvariant point the ratio of F_2 to O_2 fugacity becomes fixed. The final stages of crystallization of Martian and lunar basalts would have taken place close to this pseudoinvariant point. Phosphate textures in the Los Angeles meteorite (see photomicrographs and discussions of textural relations in Greenwood et al., 2003 and Warren et al., 2004) appear to be consistent with this interpretation.

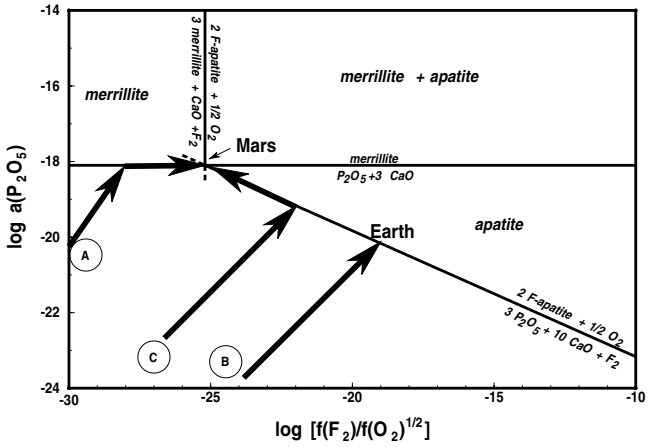

Fig. 9. Isothermal and isobaric phase diagram showing saturation of phosphate minerals as a function of phosphorus activity and the ratio between fluorine and oxygen fugacities. The diagram is calculated for end-member fluorapatite at 900 °C and 1 kbar. It is intended to show possible crystallization paths qualitatively, but not the actual values of the intensive variables in any particular sample. Paths A and B are likely phosphate crystallization paths in Mars (and the Moon) and Earth, respectively. Path C is a possible but unlikely Martian path (see text).The phase diagram for chlorapatite is qualitatively identical, as is the one for hydroxyapatite, with the exception that saturation of the latter end-member is independent of oxygen fugacity, so that the horizontal axis in that case represents fugacity of H_2O only.

Path B in Fig. 9 represents a possible crystallization path for terrestrial magmas, in which whitlockite (the terrestrial equivalent of merrillite) is unreported, except for one possible occurrence in a late-magmatic vein (Griffin et al., 1972). In terrestrial magmas apatite crystallizes first. If the silicate-oxide assemblage buffers lime activity and oxygen fugacity and no other phosphate or halogen-bearing phases are present then the system remains on the apatite phase boundary. Crystallization of apatite in this case could cause the system to slide up or down along this phase boundary, depending on P_2O_5/F_2 partitioning between apatite and melt. Changes in oxygen fugacity would have the same effect, with oxidation (the likely result of fractionation of Fe^{2+}-bearing silicate phases) displacing the system in the direction of merrillite saturation. Devolatilization would also move the system towards merrillite saturation. The effect of volatile loss, however, is probably much smaller for fluorine than for chlorine or water, given fluorine's strong affinity for silicate melt (e.g. Candela, 1986; Carroll and Webster, 1994). The fact that merrillite saturation never occurs in terrestrial magmas must mean that these magmas always reach the apatite phase boundary at volatile fugacities that are high enough relative to the pseudoinvariant point that the sum of all of these effects (apatite fractionation, oxidation and degassing) is never sufficient to raise P_2O_5 activity to that required for merrillite crystallization.

In contrast to fluorine, $\Delta \log f(Cl_2)_{QFM}$, see Fig. 7, and $\Delta \log f(H_2O)$, see Fig. 8, vary over ranges of 2–3 orders of magnitude in the Moon and ~1 order of magnitude in Mars. These ranges are wider than the estimated uncertain-

ty intervals (Appendices C and D). The different behaviors of $\Delta\log f(F_2)_{QFM}$ and $\Delta\log f(Cl_2)_{QFM}$ show that the spread in $\Delta\log f(Cl_2)_{QFM}$ cannot be an effect of uncertainties in lime activity, temperature and/or pressure, as changes in these variables would affect $\Delta\log f(F_2)_{QFM}$ in an identical manner. Our interpretation of the greater variability of chlorine and water fugacities is that, when apatite crystallizes because fluorine fugacity attains some critical value (Fig. 9), it locks in a record of whatever chlorine and water fugacities existed at that time. These fugacities may be subsequently modified, for example, if a vapor phase is exsolved, but fluorine fugacity (which controls apatite stability) is unlikely to change much during vapor exsolution. The ranges in chlorine and water fugacities for the Moon and Mars are distinct, with some overlap between $\Delta\log f(H_2O)$ values (Fig. 8) and a gap of more than one order of magnitude between lunar and Martian chlorine fugacities (ignoring EETA79001,357, see Fig. 7). Lunar rocks in general appear to be more strongly depleted in Cl_2 than H_2O compared to Martian meteorites (Fig. 10), although a strict comparison requires that the effect of different oxygen fugacities between the two planets be removed (see below). Compared to other lunar samples, mare basalts tend to be strongly depleted in chlorine (typically, $\Delta\log f(Cl_2)_{QFM}$ ~2 orders of magnitude lower), but not in fluorine (e.g., Fig. 7).

The pattern of variation of halogen fugacities in chondrites and acapulcoites is clearly different from those of the Moon and Mars. In primitive meteorites there is a negative correlation between fluorine and chlorine fugacities (Fig. 7), which simply arises from the fact that in many of these meteorites F + Cl almost completely fills the anion site in apatite (Fig. 1). What is significant, though, is that the constancy in F fugacities characteristic of the Moon and Mars is not observed among chondrites and their relatives (Fig. 7), which display significant variations in calculated halogen fugacities even within a single meteorite (Table 2). This behavior reflects the unequilibrated nature of primitive solar system materials and constitutes a counterexample that provides circumstantial evidence in favor of our interpretation of the constancy of calculated fluorine fugacities in the Moon and Mars.

The constancy of fluorine fugacities at apatite saturation (in those cases in which apatite crystallized at equilibrium with merrillite) suggests that fluorine fugacities can be used as a reference to compare volatile fugacity ratios among the terrestrial planets. This can be quantified by introducing the variables $\Delta\log f(Cl_2)_{F_2}$ and $\Delta\log f(H_2O)_{F_2}$, as follows:

$$\begin{aligned}\Delta\log f(Cl_2)_{F_2} &= \Delta\log f(Cl_2)_{QFM} - \Delta\log f(F_2)_{QFM}\\ \Delta\log f(H_2O)_{F_2} &= \Delta\log f(H_2O) - \Delta\log f(F_2)_{QFM}\end{aligned} \quad (11)$$

These variables are equal to the log of the ratio of the (respective) *absolute* volatile fugacities plus a term that is a function of the temperature at which apatite crystallized (see Appendix F for details). Because the activity of merrillite cancels out in these expressions, the values of these

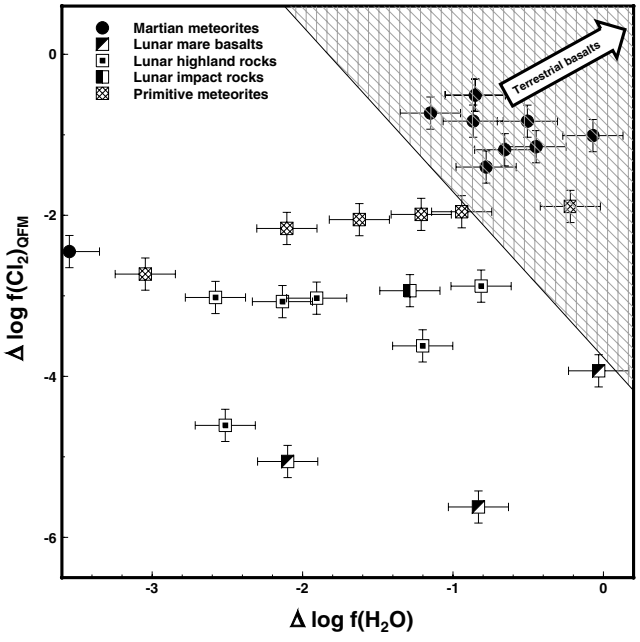

Fig. 10. Relationship between relative chlorine and water fugacities. Details as for Fig. 7.

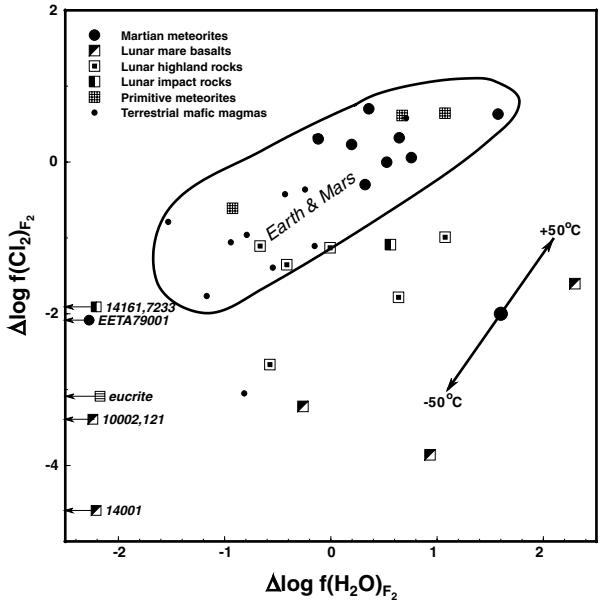

Fig. 11. Relationship between chlorine and water fugacities normalized to fluorine fugacities (Eq. (11) and Appendix F). Values for terrestrial mafic magmas are in this case actual values (not lower bounds) because merrillite activity vanishes in the definition of the variables $\Delta\log f(Cl_2)_{F_2}$ and $\Delta\log f(H_2O)_{F_2}$. Most terrestrial and Martian samples define a broad positively sloping trend that also includes chondritic meteorites, with Martian samples on the high end of the trend. Lunar rocks are more widely scattered but appear to record Cl_2/H_2O fugacity ratios that are consistently lower than those of Mars and the Earth. Chlorine depletion is particularly strong in mare basalts. The double arrow shows the effect of uncertainties in apatite saturation temperatures. Samples identified with their numbers on the left axis have calculated $\Delta\log f(H_2O)_{F_2}$ values lower than −2.5, but are shown on their correct $\Delta\log f(Cl_2)_{F_2}$ coordinate.

variables for Earth, Moon, Mars and primitive meteorites (shown in Fig. 11) are directly comparable to one another, regardless of whether or not merrillite crystallized at equilibrium with apatite in any given sample. Variations in apatite crystallization temperatures will cause the variables to move along the double arrow shown in Fig. 11 (the length of the double arrow corresponds to a total temperature range of 100 °C). Oxygen fugacity differences vanish in the definition of $\Delta \log f(Cl_2)_{F_2}$, whereas the definition of $\Delta \log f(H_2O)_{F_2}$ contains the oxygen fugacity of the QFM buffer, which is also a function of temperature (see Appendix F).

Taken together, $\Delta \log f(Cl_2)_{F_2}$ and $\Delta \log f(H_2O)_{F_2}$ for samples from Mars, Earth and primitive meteorites define a positively sloping field in Fig. 11. This correlation can reflect both temperature differences among the samples and the fact that Cl_2 partitions strongly into hydrous fluids coexisting with silicate melts, (whereas F_2 partitions into the melt, e.g., Carroll and Webster, 1994), but the relative magnitude of each of these effects cannot be ascertained without precise temperature constraints. The fact that Martian and terrestrial samples plot along the same general trend, however, means that the ratio of Cl_2 to H_2O fugacities in samples from the two planets must be similar. The fact that terrestrial samples are on the lower end of the trend relative to Martian samples could mean either that the ratios of F_2 fugacity to Cl_2 and H_2O fugacities are higher in terrestrial samples than in Martian samples or that apatite always crystallizes at lower temperature in Earth than in Mars (see Eqs. (11) and Appendix F). These observations are discussed more fully in the next section.

In contrast to the Earth–Mars trend, lunar rocks are scattered in Fig. 11. Although values of $\Delta \log f(H_2O)_{QFM}$ in lunar rocks are highly uncertain (because anion deficiency in lunar apatites is always small), some observations appear to be robust. Most lunar rocks have lower values of $\Delta \log f(Cl_2)_{F_2}$ for a given $\Delta \log f(H_2O)_{F_2}$ than Martian and terrestrial rocks, but chlorine depletion is particularly strong in mare basalts (the only exception is the lunar meteorite La Paz Icefield 02205). In contrast, highland rocks that suffered shock metamorphism do not appear to have suffered significant loss of chlorine or water compared to other highland rocks. The eucrite sample recalculates without H_2O in apatite but the value of $\Delta \log f(Cl_2)_{F_2}$ for the eucrite (shown in Fig. 11) is comparable to that of lunar mare basalts, and definitely below values characteristic of the Earth and Mars. Chlorine fugacities in the Moon and eucrite parent body must have been vanishingly small, which is consistent with the strong Cl depletion inferred for the Moon and eucrite parent body (Ringwood and Kesson, 1977, see also Fig. 2). Experimental evidence suggests that Cl solubility in silicate melts varies directly with the Cl_2/H_2O ratio of the melt (Carroll and Webster, 1994). If this is the case then there could be a positive feedback mechanism that reinforces Cl depletion during extreme volatile loss: once the Cl_2/H_2O ratio of a melt starts decreasing it may lead to progressively faster Cl depletion. This may have happened during eruption of basalts in the lunar maria and on the surface of the eucrite parent body.

5. Conclusions

A comparison of the halogen and water fugacities of Martian and terrestrial magmas suggest some remarkable similarities and also some crucial differences between the volatile histories of the two planets. The Moon, which is known to have undergone near total volatile loss, provides a valuable reference to unravel the differences between Earth and Mars. The fact that Mars and Earth follow the same trend in terms of their $\Delta \log f(Cl_2)_{F_2}$ vs. $\Delta \log f(H_2O)_{F_2}$ values (Fig. 11) means that, as long as fugacities at apatite saturation are related in a consistent way to mantle source fugacities, then the ratio of $f(Cl_2)$ to $f(H_2O)$ is broadly the same in the mantles of the Earth and Mars. In other words, if the mantle of one of the two planets is wetter than the other, then it is also richer in Cl_2. The variables plotted in Fig. 11 cannot address the issue of *absolute* fugacity values, but phosphate phase relations can (Fig. 9). The most straightforward explanation for the observation that Martian basalts are almost without exception saturated with merrillite, whereas terrestrial basalts are not, is that halogen and water fugacities are higher in the terrestrial mantle. Note that even if merrillite crystallization in Mars occurred after apatite crystallization, for example, along a path such as C in Fig. 9, such a path will almost certainly be located to the left of possible terrestrial paths. This is so because the higher P content of Martian basalts compared to terrestrial basalts (e.g., Basaltic Volcanism Study Project, 1981) must be reflected in a higher P_2O_5 activity in Martian magmas. If Martian magmas attain apatite saturation at lower halogen to oxygen fugacity ratios than terrestrial magmas, and they are more reduced than terrestrial magmas, then halogen fugacity must also be lower.

The importance of this conclusion is that it allows us to address an outstanding issue regarding the nature of the Martian mantle. McSween and co-workers (e.g., McSween et al., 2001) have argued in favor of a wet Martian mantle, on the basis of B and Li depletion profiles in SNC pyroxenes. Most other investigators (e.g., Dreibus and Wänke, 1987; Wänke and Dreibus, 1994; Watson et al., 1994; Jones, 2004b) contend that the Martian mantle is dry, largely on the basis of the low bulk H_2O content of SNC's, the extreme rarity of hydrous phases in them, and the low H_2O contents of the (rare) nominally hydrous SNC silicate phases (but not of apatite, Watson et al., 1994; McCoy et al., 1999). Dreibus and Wänke (1987), however, have also suggested that the Martian mantle is perhaps as Cl rich as the terrestrial mantle, on the basis of the observation that SNC's have K/Cl ratios comparable to those of MORB's and OIB's (see also Figs. 2 and 3). Our analysis shows that *the Martian mantle parental*

to SNC meteorites was both dry and poor in Cl compared to the terrestrial mantle. We see no simpler way of reconciling the observations summarized in Figs. 9 and 11. We argue that the high Cl contents measured in some SNC's (reflected in Figs. 2 and 3) arise from the presence of chlorine-bearing phases of secondary origin, which have been described in some SNC's and interpreted as the result of either post-eruptive evaporite deposition on the Martian surface (Bridges and Grady, 1999; Wentworth et al., 2000) or assimilation of evaporite lithologies by Martian magmas (Bridges and Grady, 1999). We contend that high bulk Cl contents in SNC's do not reflect high mantle Cl fugacities at the time of magma generation, *and that the Cl budget of the Martian mantle is more accurately reflected in the relatively low Cl fugacities recorded by apatite–merrillite pairs*.

The fact that the Martian mantle parental to SNC's was poor in Cl does not mean that this was always the case. Lodders and Fegley (1997) estimate, on the basis of isotopic mass balance, that the primordial Martian mantle was significantly richer in Cl than the mantle from which shergottites originated, so that most Cl must have been transferred to the planet's surface early on, most likely dissolved in hydrous fluids during initial crust formation. The limited data available show remarkably little variability in halogen and water fugacities throughout almost 4 billion years of the planet's history, from ALH84001, through Lafayette to the basaltic shergottites (Figs. 7, 8 and 10). Our analysis shows no evidence for significant volcanic outgassing of Mars over that period of time, supporting Lodders and Fegley's (1997) contention that the volatile inventory of the Martian mantle was "frozen in" early on, most probably prior to 4 billion years ago. Lacking plate tectonics, halogens and water could not return to the Martian mantle. The high Cl and Br contents of the Martian surface (Gellert et al., 2004; Rieder et al., 2004) are a consequence of early planetary degassing and not of protracted volcanic activity.

In contrast to Mars, at least some halogens and water have returned to the terrestrial mantle via subduction (see also Jones, 2004b), and subduction is probably also responsible for an additional observation. This is the fact that the Earth's mantle has lower H_2O/F_2 and Cl_2/F_2 fugacity ratios than the Martian mantle, as suggested by the fact that terrestrial data points in Fig. 11 plot at the lower end of the Mars–Earth trend (alternatively, one would have to accept that apatite crystallizes at consistently lower temperatures in the Earth than in Mars, which goes against the F/Cl and F/H_2O enrichment of terrestrial apatite suggested by this same figure). Terrestrial basalts also have higher bulk F contents than SNC's (Fig. 2). Given that the F end-member of hydrous silicates tends to be the most thermally stable component, devolatilization of the subducting plate under magmatic arcs may generate F-rich residues that are eventually incorporated into the mantle (Straub and Layne, 2003), enriching the Earth's mantle in fluorine throughout geologic time.

A distinctive feature of volatile fugacities in lunar rocks is that they suggest that the Moon is strongly depleted in chlorine, in absolute terms (Ringwood and Kesson, 1977) and also perhaps with respect to water (Fig. 11), and that this depletion is most extreme in mare basalts. These conclusions must be regarded with caution, as they rely on hydroxyl contents in apatite estimated by difference, and must be substantiated by direct H analyses in lunar apatites. If the relative volatile depletions tentatively observed in the Moon ($Cl_2 > H_2O > F_2$) are true, then they were intensified during eruptive processes characteristic of mare basalt volcanism, post-dating the lunar magma ocean. Analogues of this process in the other terrestrial planets appear to be missing.

Acknowledgments

Allan Treiman reviewed an earlier version of this manuscript and provided constructive criticism that was very helpful in improving the paper. An anonymous reviewer and, most especially, Bradley Jolliff provided very constructive criticism of this version, which helped us correct some misconceptions and further improve the paper.

Associate editor: Alan D. Brandon

Appendix A. Thermodynamic relations

The thermodynamic equilibrium condition for reaction 1-F (used as an example) can be written in its most general form as:

$$\Delta G^{P,T} = \Delta G^{I,T} + (P-1)\Delta V_{\text{solids}} + RT\ln K_{\text{F-phosphates}} + RT\ln a(\text{CaO}) + RT\ln f(\text{F}_2) - \frac{1}{2}RT\ln f(\text{O}_2) = 0 \quad \text{(A.1)}$$

where $\Delta G^{P,T}$ and $\Delta G^{1,T}$ are the Gibbs free energy changes of reaction 1-F at the pressure and temperature of interest, and at 1 bar and the temperature of interest, respectively, and ΔV_{solids} is the change in molar volume between the solids in the reaction (merrillite, apatite and lime, for all of which the standard state is taken to be the pure solid at the temperature and pressure of interest—it will be shown below that the choice of standard state is unimportant). The terms $a(\text{CaO})$, $f(\text{F}_2)$ and $f(\text{O}_2)$ are the activity of lime and the fugacities of fluorine and oxygen under which the apatite–merrillite assemblage crystallized, and the equilibrium constant is given by Eq. (3), in which $a(Ca_3(PO_4)_2)_{me}$ and $a(Ca_5(PO_4)_3F)_{ap}$ are the activities of $Ca_3(PO_4)_2$ and $Ca_5(PO_4)_3F$ in merrillite and apatite solid solutions, respectively.

Whereas Eq. (A.1) describes equilibrium of any arbitrary apatite–merrillite assemblage, we can also consider equilibrium among pure end-member fluorapatite and merrillite at the same pressure, temperature and $a(\text{CaO})$ at

which an assemblage of interest crystallized, and at an arbitrarily chosen oxygen fugacity. We call the fluorine and oxygen fugacities required for equilibrium of this end-member assemblage the reference fugacities, $f(F_2)_{ref}$ and $f(O_2)_{ref}$. Given that phosphate activities are now unity, the equilibrium condition for the end-member assemblage is:

$$\Delta G^{P,T} = \Delta G^{I,T} + (P-1)\Delta V_{solids} + RT\ln a(CaO) + RT\ln f(F_2)_{ref} - \frac{1}{2}RT\ln f(O_2)_{ref} = 0 \quad (A.2)$$

Subtracting Eq. (A.2) from Eq. (A.1) and dividing by RT yields:

$$\ln K_{F\text{-phosphates}} + \ln f(F_2) - \ln f(F_2)_{ref} - \frac{1}{2}[\ln f(O_2) - \ln f(O_2)_{ref}] = 0 \quad (A.3)$$

We take the log relative fluorine and oxygen fugacities, $\Delta\log f(F_2)$ and $\Delta\log f(O_2)$, measured with respect to the reference fugacities of the end-member assemblage given by Eq. (A.2):

$$\Delta\log f(F_2) = \log f(F_2) - \log f(F_2)_{ref}$$
$$\Delta\log f(O_2) = \log f(O_2) - \log f(O_2)_{ref} \quad (A.4)$$

and, converting Eq. (A.3) to decimal logarithms and substituting Eqs. (A.4) we obtain:

$$\Delta\log f(F_2) = \frac{1}{2}\Delta\log f(O_2) - \log K_{F\text{-phosphates}} \quad (A.5)$$

Choosing the QFM oxygen buffer as the reference, we get (at fixed P and T):

$$\Delta\log f(O_2)_{QFM} = \log f(O_2)_{sample} - \log f(O_2)_{QFM} \quad (A.6)$$

which leads to:

$$\Delta\log f(F_2)_{QFM} = \frac{1}{2}\Delta\log f(O_2)_{QFM} - \log K_{F\text{-phosphates}} \quad (A.7)$$

Equation (A.7, or 2 in the main text) gives the relative fluorine fugacity under which a given apatite–merrillite assemblage crystallized (characterized by its specific value of $K_{F\text{-phosphates}}$), measured with respect to the fluorine fugacity for equilibrium between pure end-member fluorapatite and merrillite at the same pressure, temperature and lime activity as the assemblage of interest, and at the oxygen fugacity of the QFM buffer for that pressure and temperature. Note that because the chemical potential of lime vanishes in these equations, the choice of a standard state for CaO is irrelevant.

Appendix B. Phosphate activity–composition relationships

Although both apatite and merrillite are nominally Ca phosphates, Ca mole fractions in both phases are commonly less than 1, and sometimes significantly so. Fe, Mg, Mn, Sr, Na and REE substitute for Ca in both apatite (Rønsbo, 1989; Deer et al., 1992; Jolliff et al., 1993) and merrillite (Jolliff et al., 1993; Rubin, 1997; Sha, 2000), although substitution appears to be more extensive in the latter than in the former. Additionally, in apatite there is mixing between F, Cl and OH in the anion site. Previous studies of apatite solid solution (Tacker and Stormer, 1989; Zhu and Sverjensky, 1991) suggest that apatite can be reasonably modeled as an ideal solution, especially at temperatures greater than 500 °C (i.e., at magmatic temperatures). Non-ideal mixing in merrillite may have an important effect in its uptake of trace elements (Colson and Jolliff, 1993) but is unlikely to affect the activity of its dominant Ca end-member. We have therefore treated both phosphates as ideal solutions.

Assuming that the three cation sites in merrillite and the five cation sites in apatite are equivalent, we define the activity of $Ca_3(PO_4)_2$ in merrillite as:

$$a[Ca_3(PO_4)_2]_{me} = (X_{Ca})^3 \quad (B.1)$$

and the activities of the three apatite end members as:

$$a[Ca_5(PO_4)_3F]_{ap} = (X_{Ca})^5\cdot(X_F)$$
$$a[Ca_5(PO_4)_3Cl]_{ap} = (X_{Ca})^5\cdot(X_{Cl}) \quad (B.2)$$
$$a[Ca_5(PO_4)_3OH]_{ap} = (X_{Ca})^5\cdot(X_{OH})$$

Calculated phosphate component activities for all of the samples shown in Table 1, calculated with these equations, are given in Table B.1. Although the three Ca sites in merrillite may not be equivalent, with ordering of Ca into the B sites and REE, Mg and Fe into the IIA sites (Dowty, 1977; Jolliff et al., 1993), the extent to which this ordering takes place may exhibit considerable variation, depending on the composition and conditions of formation of merrillite (Dowty, 1977). It is uncertain whether including such ordering assumptions is justified when dealing with such a wide range of samples as those discussed here. The effect of this ordering would be to lower merrillite activities relative to those calculated in Table B.1, and hence raise calculated volatile fugacities relative to those given in Table 2 (see Eqs. (2) and (3)). Given their different compositions, the effect would be somewhat stronger for lunar rocks (~+0.3 log fugacity units) than for Martian meteorites (~+0.1 log fugacity units). Another source of uncertainty could be the possible presence of minor (trace?) amounts of volatiles in merrillite. Given that the possible substitution mechanism is unknown, and that measurable volatile contents in merrillite are seldom reported, we have ignored the effect of volatiles on merrillite activity. None of these uncertainties in merrillite activity would affect the conclusions derived in this paper. In particular, because merrillite activity vanishes in the calculation of chlorine and water fugacities referenced to fluorine fugacity (Eq. (11)), Fig. 11 and the attendant discussion are completely independent of any uncertainties in merrillite activities and would thus remain unchanged.

Table B.1
Phosphate end member activities

	Apatite			Merrilite
	a(F-ap)	*a*(Cl-ap)	*a*(OH-ap)	*a*(Me)
Martian meteorites				
Los Angeles	0.281	0.300	0.337	0.683
Los Angeles (stone 2)	0.171	0.353	0.524	0.686
Zagami (low Cl)	0.297	0.296	0.272	0.696
Zagami (high Cl)	0.341	0.445	0.214	0.696
Shergotty	0.253	0.366	0.267	0.611
NWA480	0.327	0.232	0.238	0.699
Lafayette	0.375	0.491	0.000	
ALH 84001	0.240	0.539	0.182	0.617
ALH 84001	0.331	0.470	0.145	0.667
EETA 79001,357	0.640	0.061	0.008	0.640
Lunar rocks				
Mare basalts				
14053	0.877	0.021	0.036	0.551
14053	0.834	0.010	0.137	0.504
14001,7,3	0.995	0.005	0.000	0.541
10002,121	0.899	0.018	0.000	
LAP 02205	0.431	0.068	0.341	
Highland rocks				
14310	0.779	0.036	0.023	0.551
10085-LR-1	0.628	0.171	0.035	0.462
14161,7373	0.763	0.098	0.089	0.502
14161,7044	0.821	0.173	0.029	0.481
14161,7069	0.616	0.197	0.120	0.453
14161,7264	0.906	0.058	0.000	0.448
14161,7269	0.695	0.194	0.018	
14161,7350	0.886	0.098	0.000	0.448
Impact rocks				
12013,10	0.648	0.185	0.069	0.454
14161,7233	0.839	0.093	0.000	0.461
Eucrites				
Delaney et al.	0.970	0.030	0.000	
Chondrites and acapulcoites				
Seoni	0.000	0.667	0.122	0.624
Willowbar	0.000	0.739	0.178	0.652
Acapulco (high Cl)	0.427	0.425	0.000	
Acapulco (high F)	0.701	0.246	0.000	
Mnmnt Draw (high Cl)	0.287	0.581	0.047	0.651
Mnmnt Draw (high F)	0.982	0.018	0.000	0.651
Krymka (high Cl)	0.263	0.552	0.068	0.579
Krymka (high F)	0.511	0.253	0.013	0.579
Maralinga CAI inclusion	0.000	0.583	0.000	
DaG 896	0.000	0.661	0.339	0.575
Terrestrial igneous rocks				
Stillwater G2	0.448	0.275	0.273	
Stillwater G3	0.192	0.374	0.434	
Kigaplait OBZ	0.576	0.116	0.307	
Kigaplait OBZ	0.635	0.256	0.109	
Skaergard CM	0.630	0.019	0.247	
Bushveld	0.000	0.823	0.072	
Bushveld	0.000	0.858	0.109	
Great Dyke	0.415	0.116	0.348	
Sudbury	0.612	0.181	0.207	
Sudbury	0.557	0.184	0.224	
Mauna Kea xenoliths	0.842	0.129	0.000	
Mauna Kea xenoliths	0.881	0.082	0.000	
Hess Deep (high F)	0.681	0.089	0.177	

(*continued on next page*)

Table B.1 (*continued*)

	Apatite			Merrilite
	a(F-ap)	*a*(Cl-ap)	*a*(OH-ap)	*a*(Me)
Hess Deep (low F)	0.292	0.427	0.248	
Hess Deep (high H_2O)	0.410	0.271	0.310	
Hawi lavas	0.913	0.051	0.000	

Samples are arranged in the same order as in Table 1.

Appendix C. Relationships between log relative fugacities and absolute volatile fugacities

Consider two apatite–merrillite assemblages that equilibrated at the same temperature and pressure but at different oxygen fugacities and lime activities. Applying the equilibrium condition (A.1) to both samples, and subtracting one from the other, the terms $\Delta G^{1,T}$ and $(P-1)\,\Delta V_{\text{solids}}$ vanish, since P and T are assumed the same for both assemblages. Dividing the remaining terms by RT, converting to decimal logarithms and rearranging yields:

$$\begin{aligned}\log f(\mathrm{F_2})_1 - \log f(\mathrm{F_2})_2 = {} & \left[\tfrac{1}{2}\log f(\mathrm{O_2})_1 - \log \mathrm{K}_{\text{F-phosphates},1}\right] \\ & - \left[\tfrac{1}{2}\log f(\mathrm{O_2})_2 - \log \mathrm{K}_{\text{F-phosphates},2}\right] \\ & - \log\left[\frac{a(\mathrm{CaO})_1}{a(\mathrm{CaO})_2}\right] \end{aligned} \tag{C.1}$$

where the subscripts 1 and 2 identify the two assemblages. Combining Eqs. (A.4) and (A.5) and rearranging we obtain:

$$\begin{aligned}&\frac{1}{2}\log f(\mathrm{O_2})_2 - \log \mathrm{K}_{\mathrm{F-phosphates}} \\ &\quad = \Delta \log f(\mathrm{F_2}) + \frac{1}{2}\log f(\mathrm{O_2})_{\text{ref}}\end{aligned} \tag{C.2}$$

If a constant oxygen fugacity reference is used (e.g., the QFM buffer reaction), then upon substituting Eq. (C.2) into Eq. (C.1) the term $1/2\log f(\mathrm{O_2})_{\text{ref}}$ cancels out (as P and T are assumed the same for both assemblages), yielding:

$$\begin{aligned}\log f(\mathrm{F_2})_1 - \log f(\mathrm{F_2})_2 = {} & \Delta \log f(\mathrm{F_2})_{\text{QFM},1} \\ & - \Delta \log f(\mathrm{F_2})_{\text{QFM},2} \\ & - \log\left[\frac{a(\mathrm{CaO})_1}{a(\mathrm{CaO})_2}\right]\end{aligned} \tag{C.3}$$

which is Eq. (8) in the main text. This relationship is also true for log relative H_2O fugacities, as there is no $\log f(O_2)$ term in Eq. (6), that defines this quantity.

In order to evaluate the uncertainty introduced by inter-sample variations in lime activity we calculated lime activities in some of the samples used to estimate volatile fugacities, by means of the following equilibria among clinopyroxene, silica and either orthopyroxene or olivine, and using both the Fe and Mg end-members:

$$\begin{aligned}&2\mathrm{CaFeSi_2O_6} \rightleftharpoons \mathrm{Fe_2SiO_4} + 3\mathrm{SiO_2} + 2\mathrm{CaO} \\ &2\mathrm{CaFeSi_2O_6} \rightleftharpoons 2\mathrm{FeSiO_3} + 2\mathrm{SiO_2} + 2\mathrm{CaO}\end{aligned} \tag{C.4}$$

Most of the lunar and Martian samples listed in Table 1 contain at least one of these assemblages. Calculated lime activities (at a constant temperature of 1000 °C) are listed in Table C.1. The table shows activities calculated from the Fe and Mg end-members of each reaction, as well as the means of those values. Calculations were done with standard state thermodynamic properties from Berman (1988 and 1996 electronic update) and assuming ideal mixing in olivine and pyroxenes. We tried using non-ideal solution models for the silicate phases (e.g., Sack and Ghiorso, 1989, 1994) and concluded that this has no significant advantage, as the excess mixing energies of olivine and pyroxene (Eqs. (C.4)) tend to cancel each other out, result-

Table C.1
Calculated lime activities at $T = 1000$ °C

	log *a*(CaO) ol/cpx (Fe)	log *a*(CaO) ol/cpx (Mg)	log *a*(CaO) opx/cpx (Fe)	log *a*(CaO) opx/cpx (Mg)	log *a*(CaO) mean
Martian meteorites					
Los Angeles	−4.06	−4.23			−4.14
Zagami	−3.98	−4.03			−4.00
Shergotty			−4.20	−4.16	−4.18
NWA480			−4.07	−4.23	−4.15
Lafayette	−4.26	−4.22			−4.24
ALH 84001			−3.97	−4.24	−4.10
Lunar rocks					
14310	−4.35	−4.07			−4.21
12013,10			−3.85	−4.28	−4.06
10085-LR-1			−3.93	−4.37	−4.15
14161,7373			−3.95	−4.22	−4.08

ing in differences in the calculated lime activities (Table C.1) of less than 10% relative to the values calculated assuming ideal mixing. Table C.1 also shows that in most cases the difference between lime activities calculated from the Fe and Mg end-members is small, providing an additional justification for the assumption of ideal olivine and pyroxene activities. Finally, it must be remembered that what we are interested in is a *ratio* between lime activities (Eq. (C.3)), rendering any accuracy gain that could be obtained from using non-ideal solution models even less significant. The log value for the ratio of maximum to minimum calculated lime activities (see Eq. (C.3) and Table C.1) is 0.23.

Appendix D. Analytical uncertainties

The compositional data that we have used come from a large number of different sources, spanning more than three decades and multiple analytical facilities (see Table 1). In most cases, moreover, analyses lack replications (or at least the latter were not reported). A formal assessment of analytical uncertainties appears to be impossible. In order to generate an estimate of the likely effects of analytical uncertainties on calculated fugacities we have assumed that halogen analyses carry an uncertainty of ± 20 wt% relative, and then applied this uncertainty to the apatite composition in the Los Angeles meteorite, which contains comparable molar proportions of the three end-members (Table 1). We calculated six fictitious stoichiometries for the Los Angeles apatite, spanning a possible range of compositions given by our assumed analytical uncertainty. In each of the six fictitious stoichiometries one of the volatile components had the concentration reported by Greenwood et al. (2003), whereas the other two had concentrations 20% higher and lower, respectively, than those reported by these authors. We then calculated $\Delta\log f(F_2)$, $\Delta\log f(Cl_2)$ and $\Delta\log f(H_2O)$ for each of the fictitious stoichiometries. The resulting values were within ±0.2 log units (for F_2), ±0.18 log units (for Cl_2) and ±0.15 log units (for H_2O) of the values reported in Table 2. We take the greatest of these ranges (±0.2 log units) as an estimate of the likely effect of halogen analytical uncertainties on all calculated log relative volatile fugacities. The other possible source of analytical uncertainty would be derived from CaO analyses. However, given the very high Ca concentrations in both apatite and merrillite, this is likely to be much smaller than uncertainties derived from halogen analyses and we will consequently ignore it. Note that analytical uncertainties would affect calculations of absolute fugacities to the same extent that they affect log relative fugacities.

Appendix E. Fugacities at apatite saturation and mantle source fugacities

Halogens and water in basaltic melts are dilute solutions so that it is reasonable to assume that they follow Henry's law. The fugacity of a dilute volatile species (e.g., a halogen or water in a silicate melt), a, at any given combination of pressure and temperature conditions (that we can label "conditions *i*") is given by:

$$f_a^i = k_a^i \cdot X_a^i \cdot f_a^{o,i} \tag{E.1}$$

where X^i_a is the mole fraction of species *a*, k_a^i is Henry's law constant (e.g., for dissolution of species *a* in a silicate melt) at conditions *i*, and $f_a^{o,i}$ is the standard state fugacity of pure a at the pressure and temperature conditions labeled *i*. If we now consider any other arbitrary combination of pressure and temperature, which we will label "conditions *s*", at which the mole fraction of volatile a has changed by a factor *R* relative to conditions *i*, then the ratio of the fugacity of volatile a at conditions *i* to the fugacity of volatile a at conditions *s* is given by:

$$\frac{f_a^i}{f_a^s} = \frac{k_a^i}{k_a^s} \cdot \frac{1}{R} \cdot \frac{f_a^{o,i}}{f_a^{o,s}} \tag{E.2}$$

If we now consider two different volatile species, *a* and *b*, undergoing the same change in pressure and temperature conditions, from *i* to *s*, and such that the concentrations of both volatiles change by the same factor *R* (e.g., during closed system fractionation without separation of volatile-bearing phases), then upon dividing Eq. (E.2) by the corresponding equation for volatile species *b*, and rearranging, we obtain:

$$\frac{f_a^i}{f_b^i} = \frac{f_a^s}{f_b^s} \cdot \left[\frac{k_a^i/k_a^s}{k_b^i/k_b^s}\right] \cdot \left[\frac{f_a^{o,i}/f_a^{o,s}}{f_b^{o,i}/f_b^{o,s}}\right] \tag{E.3}$$

which is Eq. (10) in the main text.

Appendix F. Fluorine fugacities as the reference for chlorine and water fugacities

Starting from the definition of $\Delta\log f(F_2)$, given by Eq. (A.4), taking the reference oxygen fugacity to be the QFM buffer, and constructing the equivalent expression for $\Delta\log f(Cl_2)$, one gets:

$$\begin{aligned}\Delta\log f(F_2)_{QFM} &= \log f(F_2) - \log f(F_2)_{QFM}\\ \Delta\log f(Cl_2)_{QFM} &= \log f(Cl_2) - \log f(Cl_2)_{QFM}\end{aligned} \tag{F.1}$$

substituting into Eq. (11) yields:

$$\Delta\log f(Cl_2)_{F_2} = \log\left[\frac{f(Cl_2)}{f(F_2)}\right] - \log\left[\frac{f(Cl_2)_{QFM}}{f(F_2)_{QFM}}\right] \tag{F.2}$$

The second term in this equation is the ratio of halogen fugacities given by the exchange reaction:

$$2\ \text{chlorapatite} + F_2 = 2\ \text{fluorapatite} + Cl_2 \tag{F.3}$$

between end-member solids at the pressure and temperature of interest. Similarly,

$$\Delta\log f(H_2O)_{F_2} = \log\left[\frac{f(H_2O)}{f(F_2)}\right] - \log\left[\frac{f(H_2O)}{f(F_2)_{QFM}}\right] \tag{F.4}$$

where the second term is the ratio of water to fluorine fugacity defined by the following reaction between end-member solids, at the pressure and temperature of interest and the oxygen fugacity of the QFM buffer:

$$2\ \text{hydroxyapatite} + F_2 = 2\ \text{fluorapatite} + H_2O + \frac{1}{2}O_2 \qquad \text{(F.5)}$$

Each of the variables defined by Eq. (11) is thus equal to the ratio of the respective absolute fugacities plus a term that is a function of temperature and pressure only. Note that $f(O_2)$ vanishes in the $\Delta \log f(Cl_2)_{F_2}$, and that the only oxygen fugacity that enters into $\Delta \log f(H_2O)_{F_2}$ is $f(O_2)$ of the QFM buffer, which is a function of temperature and pressure only. Uncertainties in apatite crystallization temperatures affect both $\Delta \log f(Cl_2)_{F_2}$ and $\Delta \log f(H_2O)_{F_2}$, so that temperature uncertainties will force the calculated values of these variables to move along the diagonal double arrow shown in Fig. 11 (the length of the arrow corresponds to a temperature uncertainty of ±50 °C). The effect of pressure uncertainties is negligible.

References

Albee, A.L., Chodos, A.A., 1970. Microprobe investigations on Apollo 11 samples. In: Levinson, A.A. (Ed.), *Proceedings of the Apollo 11 Lunar Science Conference*. Pergamon Press, New York, pp. 135–158.

Anand, M., Taylor, L.A., Floss, C., Neal, C.R., Terada, K., Tanikawa, S., 2006. Petrology and geochemistry of La Paz Icefield 02205: a unique low-Ti mare-basalt meteorite. *Geochim. Cosmochim. Acta* **70**, 246–264.

Aoki, K., Ishiwaka, K., Kanisawa, S., 1981. Fluorine geochemistry of basaltic rocks from continental and oceanic regions and petrogenetic application. *Contrib. Mineral. Petrol.* **76**, 53–59.

Barrat, J.A., Gillet, Ph., Sauter, V., Jambon, A., Javoy, M., Göpel, C., Lesourd, M., Keller, F., Petit, E., 2002. Petrology and Geochemistry of the basaltic shregottite North West Africa 480. *Meteoritics Planet. Sci.* **37**, 487–499.

Basaltic Volcanism Study Project, 1981. *Basaltic Volcanism on the Terrestrial Planets*. Pergamon Press, New York.

Beaty, D.W., Hill, S.M.R., Albee, A.L., 1979. The petrology and chemistry of basaltic fragments from the Apollo 11 soil, part I. *Proc. Lunar Planet. Sci. Conf.* **10**, 41–75.

Berman, R.G., 1988. Internally-consistent thermodynamic data for stoichiometric minerals in the system Na_2O–K_2O–CaO–MgO–FeO–Fe_2O_3–Al_2O_3–SiO_2–TiO_2–H_2O–CO_2. *J. Petrol.* **29**, 445–522.

Beswick, A.E., Carmichael, I.S.E., 1978. Constraints on mantle source compositions imposed by phosphorous and the rare-earth elements. *Contrib. Mineral. Petrol.* **67**, 317–330.

Boctor, N.Z., Alexander, C.M.O'D., Wang, J., Hauri, E., 2003. The sources of water in Martian meteorites: clues from hydrogen isotopes. *Geochim. Cosmochim. Acta* **67**, 3971–3989.

Borg, L.E., Nyquist, L.E., Wiesmann, H., Chih, C.-Y., Reese, Y., 2003. The age of Dar al Gani 476 and the differentiation history of the Martian meteorites inferred from their radiogenic isotopic systematics. *Geochim. Cosmochim. Acta* **67**, 3519–3536.

Boudreau, A.E., McCallum, I.S., 1989. Investigation of the Stillwater Complex: part V. Apatites as indicators of evolving fluid composition. *Contrib. Mineral. Petrol.* **102**, 138–153.

Boudreau, A.E., Love, C., Prendergast, M.D., 1995. Halogen geochemistry of the Great Dyke, Zimbabwe. *Contrib. Mineral. Petrol.* **122**, 289–300.

Brearly, A.J., Jones, R.H., 1998. Chondritic meteorites. In: *Planetary Materials*. In: Papike, J.J. (Ed.), *Reviews in Mineralogy*, vol. 36. Mineral. Soc. Am., Washington, DC, pp. 3.1–3.398.

Bridges, J.C., Grady, M.M., 1999. A halite–siderite–anhydrite–chlorapatite assemblage in Nakhla: mineralogical evidence for evaporites on Mars. *Meteoritics Planet. Sci.* **34**, 407–415.

Brown, G.M., Peckett, A., 1977. Fluorapatites from the Skaergaaard intrusion, East Greenland. *Mineral. Mag.* **41**, 227–232.

Bunch, T.E., Reid, A.M., 1975. The Nakhlites. I—petrography and mineral chemistry. *Meteoritics* **10**, 303–315.

Candela, P.A., 1986. Toward a thermodynamic model for the halogens in magmatic systems: an application to melt-vapor-apatite equilibria. *Chem. Geol.* **57**, 289–301.

Carroll, M.R., Webster, J.D., 1994. Solubilities of sulfur, noble gases, nitrogen, chlorine, and fluorine in magmas. In: Carroll, M.R., Holloway, J.R. (Eds.), *Volatiles in Magmas, Reviews in Mineralogy*, vol. 30. Mineral. Soc. Am., Washington, DC, pp. 231–280.

Colson, R.O., Jolliff, B.L., 1993. Crystal-chemistry and partitioning of REE in whitlockite. In: *Lunar Planet. Sci. XXIV*. Lunar Planet. Inst., Houston, pp. 323–324 (abstract).

Deer, W.A., Howie, R.A., Zussman, J., 1992. *An Introduction to the Rock-Forming Minerals*, second ed. Longman Scientific and Technical, Essex.

Delaney, J.S., O'Neil, C., Prinz, M., 1984. Phosphate minerals in eucrites. In: *Lunar Planet. Sci. XV*. Lunar Planet. Inst., Houston, pp. 208–209 (abstract).

Delano, J.W., 2004. Redox state of the Moon's interior. *Oxygen in the Terrestrial Planets, Lunar and Planetary Institute Contribution*, vol. 1203. Lunar Planet. Inst., Houston, p. 21 (abstract).

Dowty, E., 1977. Phosphate in Angra Dos Reis: structure and composition of the $Ca_3(PO_4)_2$ minerals. *Earth Planet. Sci. Lett.* **35**, 347–351.

Dreibus, G., Wänke, H., 1987. Volatiles on Earth and Mars: a comparison. *Icarus* **71**, 225–240.

Dreibus, G., Spettel, B., Haubold, R., Jochum, K.P., Palme, H., Wolf, D., Zipfel, J., 2000. Chemistry of a new shergottite: Sayh al Uhaymir 005. *Meteoritics Planet. Sci.* **36**, A49.

Dreibus, G., Haubold, R., Huisl, W., Spettel, B., 2003. Comparison of the chemistry of Yamato 980459 with DaG 476 and SaU 005. In: *Evolution of the Solar System: A New Perspective from Antarctic Meteorites*. Nat. Inst. Polar Res., Tokyo, pp. 19–20.

Fegley Jr., B., Lewis, J.S., 1980. Volatile element chemistry in the solar nebula: Na, K, F, Cl, Br, and P. *Icarus* **41**, 439–455.

Fodor, R.V., 2001. The role of tonalite and diorite in Mauna Kea volcano, Hawaii, magmatism: petrology of summit-region leucocratic xenoliths. *J. Petrol.* **42**, 1685–1704.

Folco, L., Bland, P.A., D'Orazio, M., Franchi, I.A., Kelley, S.P., Rocchi, S., 2004. Extensive impact melting on the H-chondrite parent asteroid during cataclysmic bombardment of the early solar system: Evidence from the achondritic meteorite Dar al Gani 896. *Geochim. Cosmochim. Acta* **68**, 2379–2397.

Gancarz, A.J., Albee, A.L., Chodos, A.A., 1971. Petrologic and mineralogic investigation of some crystalline rocks returned by the Apollo 14 mission. *Earth Planet. Sci. Lett.* **12**, 1–18.

Gellert, R., Rieder, R., Anderson, R.C., Bruckner, J., Clark, B.C., Dreibus, G., Economou, T., Klingelhofer, G., Lugmair, G.W., Ming, D.W., Squyres, S.W., D'Uston, C., Wänke, H., Yen, A., Zipfel, J., 2004. Chemistry of rocks and soils in Gusev Crater from the alpha particle X-ray spectrometer. *Science* **305**, 829–832.

Greenwood, J.P., Blake, R.E., Coath, C.D., 2003. Ion microprobe measurements of $^{18}O/^{16}O$ ratios of phosphate minerals in the Martian meteorites ALH84001 and Los Angeles. *Geochim. Cosmochim. Acta* **67**, 2289–2298.

Griffin, W.L., Åmli, R., Heier, K.S., 1972. Whitlockite and apatite from lunar rock 14310 and from Ödegården, Norway. *Earth Planet. Sci. Lett.* **15**, 53–58.

Hansteen, T.H., Gurenko, A.A., 1998. Sulfur, chlorine, and fluorine in glass inclusions in olivine and clinopyroxene from basaltic hyaloclastites representing the Gran Canaria shield stage at Sites 953 and 956. In: Weaver, P.P.E., Schmincke, H.-U., Firth, J.V., Duffield, W. (Eds.), *Proceedings of the Ocean Drilling Program, Scientific Results*, vol. 157. Ocean Drilling Program, College Station, Texas, pp. 403–410.

Harrison, T.M., Watson, E.B., 1984. The behavior of apatite during crustal anatexis: equilibrium and kinetic considerations. *Geochim. Cosmochim. Acta* **48**, 1469–1478.

Herd, C.D.K., Papike, J.J., Brearley, A.J., 2001. Oxygen fugacity of martian basalts from electron microprobe oxygen and TEM-EELS analyses of Fe–Ti oxides. *Am. Mineral.* **86**, 1015–1024.

Holloway, J.R., 1987. Igneous fluids. In: Carmichael, I.S.E., Eugster, H.P. (Eds.), *Thermodynamic Modeling of Geological Materials: Minerals, Fluids and Melts, Reviews in Mineralogy*, vol. 17. Mineral. Soc. Am., Washington, DC, pp. 211–233.

Huntington, H.D., 1979. Kiglapait mineralogy I: apatite, biotite and volatiles. *J. Petrol.* **20**, 625–652.

Jagoutz, E., Wänke, H., 1986. Sr and Nd isotopic systematics of Shergotty meteorite. *Geochim. Cosmochim. Acta* **50**, 939–953.

Jambon, A., Deruelle, B., Dreibus, G., Pineau, F., 1995. Chlorine and bromine abundance in MORB: the contrasting behavior of the Mid-Atlantic Ridge and East Pacific Rise and implications for chlorine geodynamic cycle. *Chem. Geol.* **126**, 101–117.

Jolliff, B.L., Haskin, L.A., Colson, R.O., Wadhwa, M., 1993. Partitioning in REE-saturating minerals: theory, experiment, and modelling of whitlockite, apatite, and evolution of lunar residual magmas. *Geochim. Cosmochim. Acta* **57**, 4069–4094.

Jones, J.H., 2004a. Redox conditions on small bodies. *Oxygen in the Terrestrial Planets, Lunar and Planetary Institute Contribution*, vol. 1203. Lunar Planet. Inst., Houston, p. 34 (abstract).

Jones, J.H., 2004b. The edge of wetness: the case for dry magmatism on Mars. *Lunar Planet. Sci. XXXV*. Lunar Planet. Inst., Houston, #1179 (abstract).

Jones, J.H., 2005. Isotopic constraints on the petrology of Martian meteorites. *Lunar Planet. Sci. XXXVI*. Lunar Planet. Inst., Houston, #1860 (abstract).

Kurat, G., Zinner, E., Brandstätter, F., 2002. A plagioclase-olivine-spinel-magnetite inclusion from Maralinga (CK): evidence for sequential condensation and solid-gas exchange. *Geochim. Cosmochim. Acta* **66**, 2959–2979.

Lodders, K., 1998. A survey of shergottite, nakhlite and chassigny meteorites whole-rock compositions. *Meteoritics Planet. Sci.* **33**, A183–A190.

Lodders, K., 2003. Solar system abundances and condensation temperatures of the elements. *Astrophys. J.* **591**, 1220–1247.

Lodders, K., Fegley Jr., B., 1997. An Oxygen isotope model for the composition of Mars. *Icarus* **126**, 373–394.

Lunatic Asylum, 1970. Mineralogic and isotopic investigations on lunar rock 12013. *Earth Planet. Sci. Lett.* **9**, 137–163.

Mathews, J.F., 1972. The Critical constants of inorganic substances. *Chem. Rev.* **72**, 71–100.

McCoy, T.J., Keil, K., Clayton, R.N., Mayeda, T.K., Bogard, D.D., Garrison, D.H., Huss, G.R., Hutcheon, I.D., Wieler, R., 1996. A petrologic, chemical, and isotopic study of Monument Draw and comparison with other acapulcoites: evidence for formation by incipient partial melting. *Geochim. Cosmochim. Acta* **60**, 2681–2708.

McCoy, T.J., Wadhwa, M., Keil, K., 1999. New lithologies in the Zagami meteorite: evidence for fractional crystallization of a single magma unit on Mars. *Geochim. Cosmochim. Acta* **63**, 1249–1262.

McHone, J.G., 2002. Volatile emissions from Central Atlantic Magmatic Province basalts: Mass assumptions and environmental consequences. In: Hames, W., McHone, J.G., Renne, P., Ruppel, C. (Eds.), *The Central Atlantic Magmatic Province, Am. Geophys. U. Monograph*, vol. 136. Am. Geophys. U., Washington, DC, pp. 241–254.

McSween, H.Y., Arvidson, R.E., Bell III, J.F., Blaney, D., Cabrol, N.A., Christensen, P.R., Clark, B.C., Crisp, J.A., Crumpler, L.S., Des Marais, D.J., Farmer, J.D., Gellert, R., Ghosh, A., Gorevan, S., Graff, T., Grant, J., Haskin, L.A., Herkenhoff, K.E., Johnson, J.R., Jolliff, B.L., Klingelhoefer, G., Knudson, A.T., McLennan, S., Milam, K.A., Moersch, J.E., Morris, R.V., Rieder, R., Ruff, S.W., de Souza Jr., P.A., Squyres, S.W., Wänke, H., Wang, A., Wyatt, M.B., Yen, A., Zipfel, J., 2004. Basaltic rocks analyzed by the Spirit rover in Gusev Crater. *Science* **305**, 842–845.

McSween, H.Y., Grove, T.L., Lentz, R.C.F., Dann, J.C., Holzheld, A.H., Riciputi, L.R., Ryan, J.G., 2001. Geochemical evidence for magmatic water within Mars from pyroxenes in the Shergotty meteorite. *Nature* **409**, 487–490.

Meurer, W.P., Natland, J.H., 2001. Apatite compositions from oceanic cumulates with implications for the evolution of mid-ocean ridge magmatic systems. *J. Volcan. Geotherm. Res.* **110**, 281–298.

Meyer Jr., C., 2004. *Mars Meteorite Compendium*. Lyndon B. Johnson Space Center, Houston, Texas (Also available at http://curator.jsc.nasa.gov/antmet/mmc/mmc.htm).

Michael, P.J., Cornell, W.C., 1998. Influence of spreading rate and magma supply on crystallization and assimilation beneath mid-ocean ridges: Evidence from chlorine and major element chemistry of mid-ocean basalts. *J. Geophys. Res.* **103**, 18325–18356.

Mikouchi, T., 2001. Mineralogical similarities and differences between the Los Angeles basaltic shergottite and the Asuka-881757 lunar mare meteorite. *Antarctic Meteorite Res.* **14**, 1–20.

Min, K., Farley, K.A., Renne, P.R., Marti, K., 2003. Single grain (U-Th)/He ages from phosphates in Acapulco meteorite and implications for thermal history. *Earth Planet. Sci. Lett.* **209**, 323–336.

Mittlefehldt, D.W., 1994. ALH84001, a cumulate orthopyroxenite member of the Martian meteorite clan. *Meteoritics* **29**, 214–221.

Mittlefehldt, D.W., McCoy, T.J., Goodrich, C.A., Kracher, A., 1998. Non-chondritic meteorites from asteroidal bodies. In: Papike, J.J. (Ed.), *Planetary Materials. Reviews in Mineralogy*, vol. 36. Mineral. Soc. Am., Washington, DC, pp. 4.1–4.194.

Nash, W.P., 1976. Fluorine, chlorine and OH-bearing minerals in the Skaergard intrusion. *Am. J. Sci.* **276**, 546–557.

Nash, W.P., Hausel, W.D., 1973. Partial pressures of oxygen, phosphorous and fluorine in some lunar lavas. *Earth Planet. Sci. Lett.* **20**, 13–27.

O'Reilly, S.Y., Griffin, W.L., 2000. Apatite in the mantle: implications for metasomatic processes and high heat production in Phanerozoic mantle. *Lithos* **53**, 217–232.

Rieder, R., Gellert, R., Anderson, R.C., Brückner, J., Clark, B.C., Dreibus, G., Economou, T., Klingelhöfer, G., Lugmair, G.W., Ming, D.W., Squyres, S.W., D'Uston, C., Wänke, H., Yen, A., Zipfel, J., 2004. Chemistry of rocks and soils at Meridiani Planum from the alpha particle X-ray spectrometer. *Science* **306**, 1746–1749.

Ringwood, A.E., Kesson, S.E., 1977. Basaltic magmatism and the bulk composition of the moon. II. Siderophile and volatile elments in Moon, Earth and chondrites: implications for Lunar Origin. *The Moon* **16**, 425–464.

Rønsbo, J.G., 1989. Coupled substitutions involving REEs and Na and Si in apatites in alkaline rocks from the Ilimaussaq intrusion, South Greenland, and the petrological implications. *Am. Mineral.* **74**, 896–901.

Rubin, A.E., 1997. Mineralogy of meteorite groups. *Meteoritics Planet. Sci.* **32**, 231–247.

Sack, R.O., Ghiorso, M.S., 1989. Importance of considerations of mixing properties in establishing an internally consistent thermodynamic database: thermochemistry of minerals in the system Mg_2SiO_4–Fe_2SiO_4–SiO_2. *Contrib. Mineral. Petrol.* **102**, 41–68.

Sack, R.O., Ghiorso, M.S., 1994. Thermodynamics of multicomponent pyroxenes: II. Phase relations in the quadrilateral. *Contrib. Mineral. Petrol.* **116**, 287–300.

Sato, M., 1978. Oxygen fugacity of basaltic magmas and role of gas-forming elements. *Geophys. Res. Lett.* **5**, 447–449.

Sawyer, D.J., McGehee, M.D., Canepa, J., Moore, C., 2000. Water soluble ions in the Nakhla martian meteorite. *Meteoritics Planet. Sci.* **35**, 743–747.

Semenenko, V.P., Girich, A.L., Nittler, L.R., 2004. An exotic kind of cosmic material: graphite-containing xenoliths from the Krymka (LL31) chondrite. *Geochim. Cosmochim. Acta* **68**, 455–475.

Sha, L-K., 2000. Whitlockite solubility in silicate melts: some insights into lunar and planetary evolution. *Geochim. Cosmochim. Acta* **64**, 3217–3236.

Shearer, C.K., Papike, J.J., 2004. Oxygen fugacity of lunar basalts and the lunar mantle. Range of fO_2 and the effectiveness of oxybarometers.

Oxygen in the Terrestrial Planets, Lunar and Planetary Institute Contribution, vol. 1203. Lunar Planet. Inst., Houston, p. 58 (abtsract).

Spengler, S.R., Garcia, M.O., 1988. Geochemistry of the Hawi lavas, Kohala Volcano, Hawaii. *Contrib. Mineral. Petrol.* **99**, 90–104.

Straub, S.M., Layne, G.D., 2003. The systematics of chlorine, fluorine, and water in Izu arc front volcanic rocks: implications for volatile recycling in subduction zones. *Geochim. Cosmochim. Acta* **67**, 4179–4203.

Stroncik, N.A., Haase, K.M., 2004. Chlorine in oceanic intraplate basalts: constraints on mantle sources and recycling processes. *Geology* **32**, 945–948.

Tacker, R.C., Stormer, J.C., 1989. A thermodynamic model for apatite solid solution, applicable to high-temperature geologic problems. *Am. Mineral.* **74**, 877–888.

Tacker, R.C., Stormer, J.C., 1993. Thermodynamics of mixing of liquids in the system $Ca_2(PO_4)_2$–$CaCl_2$–CaF_2–$Ca(OH)_2$. *Geochim. Cosmochim. Acta* **57**, 4663–4676.

Taylor, G.J., Warren, P., Ryder, G., Delano, J., Pieters, C., Lofgren, G., 1991. Lunar rocks. In: Heiken, G., Vaniman, D., French, B. (Eds.), *Lunar Sourcebook, a Users Guide to the Moon*. Cambridge Univ. Press, Cambridge, pp. 183–284.

Taylor, L.A., Patchen, A., Mayne, R.G., Taylor, D-H., 2004. The most reduced rock from the Moon, Apollo 14 basalt 14053: its unique features and their origin. *Am. Mineral.* **89**, 1617–1624.

Taylor, S.R., 1982. *Planetary Science: a Lunar Perspective*. Lunar and Planetary Institute, Houston, Texas.

Toplis, M.J., Libourel, G., Carroll, M.R., 1994. The role of phosphorus in crystallisation processes of basalt: an experimental study. *Geochim. Cosmochim. Acta* **58**, 797–810.

Unni, C.K., Schilling, J-G., 1978. Cl and Br degassing by volcanism along the Reykjanes Ridge and Iceland. *Nature* **272**, 19–23.

Wang, A., Kuebler, K., Jolliff, B., Haskin, L.A., 2004. Mineralogy of a Martian meteorite as determined by Raman spectroscopy. *J. Raman Spectroscopy* **35**, 504–514.

Wänke, H., Dreibus, G., 1994. Chemistry and accretion history of Mars. *Phil. Trans. R. Soc. Lond.* **A 349**, 285–293.

Wänke, H., Baddenhausen, H., Balacescu, A., Teschke, F., Spettel, B., Dreibus, G., Palme, H., Quijano-Rico, M., Kruse, H., Wlotzka, F., Begeman, F., 1972. Multielement analyses of lunar samples and some implications of the results. In: Heymann, D. (Ed.), *Proceedings of the Third Lunar Science Conference, Vol. 2, Chemical and Isotope Analyses, Organic Chemistry*. The MIT Press, Cambridge, MA, pp. 1251–1268.

Warner, S., Martin, R.F., Abdel-Rahman, A-F.M., Doig, R., 1998. Apatite as a monitor of fractionation, degassing, and metamorphism in the Sudbury Igneous Complex, Ontario. *Can. Mineral.* **36**, 981–999.

Warren, P.H., Bridges, J.C., 2005. Geochemical subclassification of shergottites and the crustal assimilation model. *Lunar Planet Sci. XXXVI*. Lunar Planet. Inst., Houston, #2098 (abstract).

Warren, P.H., Greenwood, J.P., Rubin, A.E., 2004. Los Angeles: A tale of two stones. *Meteoritics Planetary Sci.* **39**, 137–156.

Watson, L.L., Hutcheon, I.D., Epstein, S., Stolper, E.M., 1994. Water on Mars: clues from deuterium hydrogen and water contents of hydrous phases in SNC meteorites. *Science* **265**, 86–90.

Wentworth, S.J., Thomas-Kerpta, K.L., McKay, D.S., 2000. Weathering and secondary minerals in the Martian meteorite Shergotty. *Lunar Planet. Sci. XXXI*. Lunar Planet. Inst., Houston, #1888 (abstract).

Willmore, C.C., Boudreau, A., Kruger, F.J., 2000. The halogen geochemistry of the Bushveld Complex, Republic of South Africa: implications for chalcophile element distribution in the Lower and Critical Zones. *J. Petrol.* **41**, 1517–1539.

Xirouchakis, D., Draper, D.S., Schwandt, C.S., Lanzirotti, A., 2002. Crystallization conditions of Loas Angeles, a basaltic Martian meteorite. *Geochim. Cosmochim. Acta* **66**, 1867–1880.

Zhu, C., Sverjensky, D.A., 1991. Partitioning of F-Cl-OH between minerals and hydrothermal fluids. *Geochim. Cosmochim. Acta* **55**, 1837–1858.